A potent and protective human neutralizing antibody targeting a key vulnerable site of Epstein-Barr Virus

Qian-Ying Zhu
Sun Yat-sen University
Sisi Shan
Tsinghua University https://orcid.org/0000-0002-7184-6818
Jinfang Yu
Tsinghua University https://orcid.org/0000-0002-2294-0752
Si-Ying Peng
Bejing IDMO Company Limited
Cong Sun
Sun Yat-sen University Cancer Center
Yanan Zuo
School of Medicine, Tsinghua University
Shu-Mei Yan
Sun Yat-Sen University Cancer Center
Xiao Zhang
Sun Yat-sen University Cancer Center
Ziqing Yang
Tsinghua University
Lan-Yi Zhong
Sun Yat-sen University
Xuangling Shi
Tsinghua University
Su-Mei Cao
Sun Yat-sen University Cancer Center
Xinquan Wang
Tsinghua University https://orcid.org/0000-0003-3136-8070
Mu-Sheng Zeng
Sun Yat-sen University Cancer Center https://orcid.org/0000-0003-3509-5591
Linqi Zhang (zhanglinqi@tsinghua.edu.cn)
Tsinghua University https://orcid.org/0000-0003-4931-509X

Article

Keywords: EBV, human neutralizing antibody, humanized mouse model, epitope

Posted Date: January 25th, 2021

DOI: https://doi.org/10.21203/rs.3.rs-151895/v1

Version of Record: A version of this preprint was published at Nature Communications on November 16th, 2021. See the published version at https://doi.org/10.1038/s41467-021-26912-6.

A potent and protective human neutralizing antibody targeting a key vulnerable site of Epstein-Barr Virus

Qian-Ying Zhu[1,6], Sisi Shan[2,6], Jinfang Yu[3,6], Si-Ying Peng[5], Cong Sun[1], Yanan Zuo[2], Shu-Mei Yan[1], Xiao Zhang[1], Ziqing Yang[2], Lan-Yi Zhong[1], Xuanling Shi[2], Su-Mei Cao[4], Xinquan Wang[3,*], Mu-Sheng Zeng[1,*], Linqi Zhang[2,7,*]

[1]State Key Laboratory of Oncology in South China, Collaborative Innovation Center for Cancer Medicine, Guangdong Key Laboratory of Nasopharyngeal Carcinoma Diagnosis and Therapy, Sun Yat-sen University Cancer Center (SYSUCC), Guangzhou 510060, China.

[2]Comprehensive AIDS Research Center, and Beijing Advanced Innovation Center for Structural Biology, School of Medicine and Vanke School of Public Health, Tsinghua University, Beijing 100084, China.

[3]The Ministry of Education Key Laboratory of Protein Science, Beijing Advanced Innovation Center for Structural Biology, Beijing Frontier Research Center for Biological Structure, Collaborative Innovation Center for Biotherapy, School of Life Sciences, Tsinghua University, 100084 Beijing, China.

[4]State Key Laboratory of Oncology in South China, Department of Cancer Prevention Research, Sun Yat-sen University Cancer Center (SYSUCC), Guangzhou 510060, China.

[5]Bejing IDMO Company Limited, Beijing, China.

[6]These authors contributed equally to this work.

[7]Lead Contact

[*]Correspondence:

xinquanwang@mail.tsinghua.edu.cn;

zengmsh@sysucc.org.cn;

zhanglinqi@mail.tsinghua.edu.cn

ABSTRACT

Epstein-Barr virus (EBV) is associated with a range of epithelial and B cell malignancies as well as autoimmune disorders, for which there are still no specific treatments or effective vaccines. Here, we isolated EBV gH/gL-specific antibodies from an EBV-infected individual. One antibody, 1D8, efficiently neutralized EBV infection of two major target cell types, B cells and epithelial cells. In humanized mice, 1D8 provided strong protection against a high-dose EBV challenge by substantially reducing viral loads and associated tumor burden. Crystal structure analysis revealed that 1D8 binds to a key vulnerable interface between the D-I/D-II domains of the viral gH/gL protein, especially the D-II of the gH, thereby interfering with the gH/gL-mediated membrane fusion and binding to target cells. Overall, we identified a potent neutralizing antibody as a promising candidate for prophylactic and therapeutic interventions against EBV infection. The key vulnerable site also provides insights into the EBV vaccines design.

KEY WORDS: EBV, human neutralizing antibody, humanized mouse model, epitope

INTRODUCTION

Epstein-Barr virus (EBV) is the causative agent of a wide range of diseases in humans such as infectious mononucleosis and lymphoproliferative disorders, as well as epithelial and B cell malignancies including nasopharyngeal carcinoma and Burkitt's lymphoma(*1-4*). Despite decades of research, a safe and effectively vaccine against EBV still remains elusive, largely due to a lack of knowledge regarding the specificity and magnitude of immune responses required for protection(*5-8*). EBV-infected individuals produce broad and potent neutralizing antibodies that can inhibit infection of both epithelial cells and B cells *in vitro*(*9-13*). However, their specificity to viral antigens and potential mechanism of neutralization are not clear.

Recent studies on monoclonal antibodies (mAbs) revealed some of the intricate interactions between antibodies and viral surface antigens, providing critical insights into the potential targets for antibody neutralization and vaccine development(*14-18*). The reported mAbs recognize exclusively viral surface glycoproteins that work in concert in determining viral tropism and mediating viral fusion with the target cells, such as gp350, gH/gL, gB and gp42(*19-22*). Recently, gH/gL and gB, which together constitute the fusion machinery of EBV, have drawn increasing attention as newer generations of antibodies targeting this machinery demonstrate broad and potent inhibitory activity against EBV infection of both B cells and epithelial cells(*23*), as well as cross-neutralizing reactivity to related herpesviruses of non-human primate(*9, 24, 25*).

As components of the fusion machinery, gH/gL and gB demonstrate unique structural and functional features that are critical for viral entry, but they also inadvertently expose some vulnerable sites during the process, and became susceptible to antibody binding and neutralization(*26-28*). Structurally, gH/gL consists of four distinct domains named domain-I (D-I) to domain-IV (D-IV), forming an elongated structure(*29*). D-I is formed by gL and the N-terminus of gH, while D-II to D-IV are formed by the rest of gH. D-I and D-II are connected through a linker helix and form a structurally distinct groove. For viral fusion to occur, gH/gL must interact with gB, which triggers a cascade of events involving dramatic structural changes of gB from the pre- to the post-fusion conformation(*27, 28*). Mutations in the D-I and D-I/D-II interfaces of gH/gL were shown to affect the membrane fusion process, suggesting that these regions of gH/gL are important for the interaction and activation of gB(*30, 31*).

Apart from the fusion machinery, EBV infection requires additional surface glycoproteins to complete the entry process, but the involved accessory molecules are rather different between B cells and epithelial cells(*32*). For instance, EBV utilizes gp350, one of the most abundant glycoproteins on the viral envelope, to attach to the cell surface through high-affinity interaction with CD21 or CD35(*33-35*). Such attachment promotes the bridging effect of another surface glycoprotein, gp42, which inserts itself between gH/gL and human leukocyte antigen (HLA) class II, which triggers the downstream fusion machinery(*36, 37*). Interestingly, gp42 has an inhibitory effect on epithelial cell

93 infection, suggesting a different entry mechanism in B cells and epithelial
94 cells(*38*). For infection of epithelial cells, gH/gL first binds to integrin and
95 NMHC-IIA on the cell surface. The fusion machinery then interacts with
96 neuropilin 1 (NRP1) and ephrin receptor A2 (EphA2)(*39-41*), which leads to a
97 conformational transition of gB, facilitating viral fusion(*27, 42*).

98 Most of the current anti-gH/gL antibodies are of murine origin(*36, 43*). E1D1,
99 CL59 and CL40 can block epithelial cell infection but fail to efficiently neutralize
100 B cell infection(*22*). Only one human neutralizing antibody targeting gH/gL,
101 AMMO1, was recently isolated from an EBV-infected individual(*22*). AMMO1
102 can potently block infection of both B cells and epithelial cells *in vitro*. AMMO1
103 can also protect humanized mice from EBV challenge and provide sterilizing
104 immunity in macaques against oral challenge with rhesus lymphocryptovirus,
105 the EBV relative that infects rhesus macaques. These findings indicate that a
106 vaccine capable of inducing AMMO1-like neutralizing antibodies may protect
107 human from EBV infection. Cryo-electron microscopy (cryoEM) analysis of the
108 AMMO1-gH/gL-gp42 complex revealed that AMMO1 binds to an epitope
109 between D-I and D-II of gH/gL(*22*), which serves as a more precise and clear
110 target for future vaccine design and development.

111 Here, we sought to isolate more neutralizing antibodies from EBV-infected
112 individuals targeting the EBV gH/gL. After screening a large number of infected
113 individuals, we successfully isolated the anti-gH/gL antibody 1D8, which is
114 capable of efficiently neutralizing EBV infection of epithelial cells and B cells *in*

vitro. 1D8 also provided potent protection against EBV challenge in humanized mice by significantly reducing the viral loads and associated tumor burden. Using X-ray crystallography, we determined the structure of the 1D8-gH/gL complex and showed that 1D8 recognizes a key epitope located at the top of the groove between D-I and D-II of gH/gL, especially the D-II of gH. Notably, this epitope is located on the opposite side of that recognized by AMMO1 and CL40. In addition, 1D8 also significantly inhibited viral membrane fusion and gH/gL binding to epithelial cell receptor EphA2. We believe that this new vulnerable site, together with that recognized by AMMO1 and CL40, suggests that D-I and D-II represent an attractive target for the rational design of vaccines aiming to elicit antibody responses similar to these mAbs. Finally, 1D8 could also be used alone or in combination with other mAbs in prophylactic and therapeutic interventions against EBV infection either in organ transplant recipients or immunocompromised patients.

RESULTS

Isolation of human monoclonal antibodies targeting the EBV gH/gL

We first screened plasma samples from a cohort of high-risk individuals and nasopharyngeal carcinoma patients(*44, 45*) for those with the highest levels of binding and neutralizing activity. Of the 48 plasma samples screened, donor 27 from the high-risk group had antibodies with the highest affinity for gH/gL measured by ELISA, with the half-maximal effective concentration (EC50)

137 corresponding to a 6874-fold dilution (fig. S1A). The same plasma sample also
138 displayed the most potent neutralizing activity against EBV infection of HNE1
139 epithelial cells and Raji B cells, with respective half-maximal inhibitory
140 concentrations (IC50) corresponding to a 273-fold and 1250-fold dilution (fig.
141 S1B). To isolate monoclonal antibodies, we used phycoerythrin (PE)
142 conjugated gH/gL as baits to stain and sort the antigen-specific memory B cells
143 from the peripheral blood mononuclear cells (PBMCs) of donor 27 using flow
144 cytometry (Fig. 1A). Out of a total 54 sorted single B cells, we were able to
145 clone and express 10 full-length human immunoglobulin G1 (IgG1) genes in
146 transfected 293T cells. Two antibodies, 1D8 and 2A6, were found to have
147 strong binding to gH/gL. As shown in Fig. 1B, 1D8 showed ~7-fold stronger
148 binding to gH/gL than 2A6, with an EC50 of 0.008μg/ml and 0.057μg/ml,
149 respectively. 1D8 also demonstrated higher neutralizing activity than 2A6
150 against EBV infection of HNE1 epithelial cells and Raji B cells (Fig. 1C,D and
151 table S1). The IC_{50} of 1D8 was about 6 times lower than that of 2A6 for both
152 cell types. Notably, 1D8 displayed comparable binding and neutralizing
153 activities to AMMO1, a potent gH/gL-specific neutralizing antibody previously
154 isolated from an EBV-infected individual(*22*). The equilibrium dissociation
155 constant (KD) measured by SPR was 0.59nM for 1D8 and 0.14nM for AMMO1
156 (fig. S1C,D and table S2). When tested for neutralizing activity against EBV
157 infection, 1D8 and AMMO1 showed IC50 values of 0.238 and 0.318μg/ml in
158 Raji B cells, as well as 0.123 and 0.127μg/ml in HNE1 epithelial cells,

159 respectively (Fig. 1C,D and table S1).

160

161 **1D8 protects against lethal EBV challenge in humanized mice**

162 To test the protective potential of 1D8 *in vivo*, we used a humanized mouse
163 model reconstituted with human cord blood-derived CD34+ stem cells that
164 became susceptible to EBV infection and disease after approximately 8 weeks
165 of development and maturation(*46-48*). The entire experimental protocol and
166 assays conducted to evaluate protection are outlined in Fig. 2A. Briefly, we
167 administrated 400μg of 1D8, AMMO1 as positive control, or 2G4 and PBS as
168 negative controls to groups of seven to eight humanized mice via the
169 intraperitoneal (i.p.) route. On the following day, the animals were challenged
170 with 1,000 50% transforming dose (TD_{50}) Akata EBV via the intravenous (i.v.)
171 route. In the ensuing up to 6-week period, all animals received the testing
172 antibodies or PBS weekly via the i.p. route and were monitored for body weight,
173 survival, as well as various virological and immunological parameters.

174 EBV DNA in the peripheral blood measured by quantitative PCR reflected
175 the distinctions in clinical manifestation between these animals (Fig. 2B). In the
176 animals treated with 1D8 and AMMO1, EBV DNA became detectable on week
177 3 after challenge and slowly increased in the following two weeks, but no
178 animals had EBV DNA copy numbers greater than 10 copies/μl blood at week
179 5 post challenge. By contrast, in the animals treated with 2G4 and PBS, EBV
180 DNA rapidly increased from week 3 onwards after the challenge and reached

about 100-fold higher copy numbers than in the groups treated with 1D8 and AMMO1 at week 5 post-challenge (Fig. 2B). All animals in the 1D8 and AMMO1 treated groups survived the challenge and demonstrated relatively stable body weight without obvious pathology (Fig. 2C,D). By contrast, negative control animals (2G4 and PBS groups) began significantly losing weight starting on day 28 (4 weeks), succumbed to disease and had to be euthanized by day 38 after the challenge.

By the time they were ready for the protection experiments, the reconstituted animals had about 20% human CD45+ lymphocytes in the peripheral blood, nearly 90% of which were human CD20+ B cells and <1% were human CD3+ T cells (Fig. 2E-G). In addition, the dynamic change of human CD20+ B cells and CD3+ T cells in the peripheral blood was correlated with distinct pattern of disease progression between these animals. Animals in the 1D8 and AMMO1 treated groups showed a relatively slower decrease in the number of CD20+ B cells compared with the 2G4 and PBS treated groups. At the same time, the increase in the number of CD3+ T cells was slower in animals treated with 1D8 and AMMO1 compared to those treated by 2G4 and PBS (Fig. 2F,G).

Furthermore, EBV DNA copy numbers measured in the spleen, liver and kidney collected at necropsy shared a similar trend with those measured in the peripheral blood (Fig. 2H,J). The copy numbers of EBV DNA were significantly lower in the 1D8 and AMMO1 treated groups than in the 2G4 and PBS treated groups, although the copy numbers were generally higher in the spleen than in

the liver and kidney (Fig. 2H,J). Taken together, these results demonstrated that 1D8 as well as the positive control AMMO1 can significantly reduce viral replication and provide complete protection from a lethal EBV challenge.

Marked reduction in viral replication and tissue damages in the protected animals

To study the impact of protection at the tissue levels, we collected the spleen, liver and kidney of the animals at the necropsy. The most profound and visible changes were observed in the spleens. Morphologically, the spleens from the 2G4 and PBS groups were clearly enlarged with a few irregular and pale tumors across the entire surface. By contrast, the spleens in the 1D8 and AMMO1 groups were normal in size and color, without visible tumors (Fig. 3). We went on to perform histopathology analysis on the spleen sections using hematoxylin and eosin (H&E) staining, immunohistochemistry (IHC) for hCD3 and hCD20, as well as in situ hybridization for Epstein-Barr virus-encoded RNAs (EBERs) (Fig. 3). All mice treated with 2G4 or PBS presented with typically large B-cell lymphomas in the white pulp regions, which consisted of large and atypical lymphoid cells that were positive for hCD20 and EBER. They were abundant and widely distributed across the tissue sections. Morphologically their proliferations destroyed the underlying architecture of the tissue with some infiltration by hCD3+ T cells. Additionally, areas of coagulative necrosis were often present in the spleens of mice from the 2G4

and PBS groups. By contrast, in the 1D8 and AMMO1 groups, the overall tissue architecture remained largely intact, even if some atypical large transformed cells could also be seen. Among the large number of hCD20+ B cells in the white pulp areas, EBER+ cells were relatively scarce. A few hCD3+ T cells were also found scattered within. Similarly, in the hepatic and renal sections from 2G4 and PBS groups, a large number of hCD20+ and EBER+ B cells were identified, while they were rare in the 1D8 and AMMO1 groups (fig. S2). The infected cells were frequently found near the blood vessels in both the liver and kidney, likely the results of migration and seeding from the blood circulation. Collectively, these results show that 1D8 and AMMO1 can significantly reduce viral replication and tissue damage relative to 2G4 and PBS, offering an explanation for their impressive *in vivo* protection against a lethal EBV challenge.

1D8 binds to a key epitope on gH/gL

To understand the neutralizing mechanism of 1D8, we sought to determine the structure of the 1D8-gH/gL complex by X-ray crystallography. After screening nearly 100 crystals with relatively weak diffraction, we obtained a dataset with 4.2 Å resolution and solved the structure by molecular replacement (table S3). The structure showed that 1D8 bound to the interface at the top of the groove formed by D-I and D-II of gH/gL, especially the D-II of gH (Fig. 4A). 1D8 bound to the unique epitope spanning of gH/gL, which comprised residues of both gH

247 and gL, burying a surface area of 969 Å^2. CDRL1, CDRL3 and CDRH2 of 1D8
248 made practically no contribution to the binding of gH/gL. CDRL2 mainly bound
249 to 2α-2 and 2β-2. The loop between 2α-9 and 2β-11 was bound by CDRH1
250 and CDRH3. CDRH3 also bound to the loop between 2α-1 and 2β-1. The
251 heavy chain of 1D8 bound to the loop between Lα-1 and Lα-2 (Fig. 4B). To
252 identify the key residue for antibody binding, we generated a series of single
253 alanine substitutions for the contacting residues on gH/gL. Except for two
254 (L122A and C312A), the remaining 15 mutants were successfully expressed
255 and purified from the supernatant of transfected 293F cells. We then
256 performed ELISA to assess the impact of these mutants on 1D8 binding. One
257 mutant, N310A, locate in the loop between 2α-9 and 2β-11, was identified to
258 specifically reduce the binding of 1D8 but not AMMO1 (Fig. 4B and fig. S3A,B).
259 When measured by SPR, the binding affinity of 1D8 for this particular mutant
260 dropped to 31.6nM, representing more than 53-fold decrease compared to the
261 wild type gH/gL. However, no significant change of binding was found for
262 AMMO1 compared to the wild type gH/gL (fig. S3C,D and table S2). The
263 unique binding of 1D8 is further supported by superimposing the antibodies
264 with known structural information onto the same gH/gL molecule. As shown in
265 Fig. 4C,D, 1D8 bound to gH/gL at the top of the groove formed between D-I
266 and D-II, especially the D-II of gH, while AMMO1 binds the opposite side of the
267 molecule through a discontinuous epitope formed at the D-I/D-II interface. The
268 mouse-derived antibody CL40 partially overlaps with the epitope of AMMO1 by

binding to an epitope on gH at the interface between D-II and D-III(*22*). Another mouse antibody E1D1, however, only recognizes gL(*36, 43*) (Fig. 4C,D). We also used bio-layer interferometry (BLI) to confirm that 1D8 does not compete with any of these antibodies in binding to gH/gL (fig. S3E). These results indicate that 1D8 recognizes a key vulnerable site on gH/gL and provide a good rational basis for combined use with other antibodies in suppressing EBV infection.

1D8 inhibits gH/gL-mediated membrane fusion and binding to B and epithelial cells

We next studied the ability of 1D8 to inhibit gH/gL mediated membrane fusion by monitoring the fusion efficiency between the effector and target cells. Specifically, effector CHO-K1 cells expressing the gH/gL and gB fusion machinery were incubated with a saturated concentration of 1D8 or relevant controls at 37℃ for 1h before mixing at a 1:1 ratio with the target HEK293 cells. The inhibitory activity was measured 24h afterwards via the luciferase activity in the cell lysates, which only became detectable when fusion occurred. As shown in Fig. 5A-C, the effector CHO-K1 cells expressed good levels of gH/gL as measured by flow cytometry. In the presence of 1D8 or AMMO1, the fusion activity was barely measurable and similar to the background where only the effector cells were present (Fig. 5D). By contrast, incubation with the negative controls 2G4 or PBS resulted in high levels of luciferase activity

beyond one million relative light unit (RLU). In addition, we tested the ability of 1D8 to interfere with the binding of fluorescently labelled gH/gL to Raji B cells and HK1 epithelial cells, both of which are susceptible to EBV infection *in vitro*(*49, 50*). Gp42 was included in the assessment of the binding to B cells but not for the epithelial cells, since the gH/gL-gp42 complex is specifically required for B cell activation and fusion(*36*). 1D8 and relevant controls were incubated with fluorescent-labeled gH/gL at 37℃ for 1h before mixing with B cells or epithelia cells and further incubation on ice for 1h. The levels of inhibition of gH/gL-mediated binding to both cell types were measured by flow cytometry. As shown in Fig. 5E, pre-incubation with 1D8 and AMMO1 significantly reduced but did not completely abrogate gH/gL-gp42 binding to B cells. While no difference was found between the negative controls 2G4 and PBS, AMMO1 appeared to be more potent than 1D8 in interfering with the binding of gH/gL to B cells. Conversely, 1D8 seems to be more powerful than AMMO1 in inhibiting the binding of gH/gL to the epithelia cells, whereas the negative controls showed negligible effect (Fig. 5F). Lastly, we studied the ability of 1D8 to inhibit the interaction between gH/gL and EphA2, a recently identified receptor for EBV infection of epithelial cells that depends on an interaction with gH/gL(*39, 40*). Consistent with an earlier report(*22*), the interaction between EphA2-Fc and gH/gL was indeed rather weak as measured by BLI. Nevertheless, pre-incubation of gH/gL with 1D8 did result in a small and clear reduction in the interaction between gH/gL and EphA2 (Fig.

313 5G). Conversely, such an effect was not noticed for AMMO1 or 2G4 (Fig. 5H,I).
314 This may explain why 1D8 was more effective than AMMO1 in inhibiting EBV
315 infection of epithelial cells (see above), although the underlying mechanism
316 warrants further investigation. Taken together, these findings indicate that 1D8
317 as well as the positive control AMMO1 can significantly inhibit gH/gL-mediated
318 membrane fusion and binding to B and epithelial cells, either through direct
319 blocking of binding or by sterically interfering with the downstream interactions
320 required for EBV infection.
321
322 **DISCUSSION**
323 Neutralizing antibodies are the major component of protective immunity
324 against viral infection in humans(*51-53*). They exert their function by targeting
325 crucial epitopes on the viral envelope glycoproteins. Identifying the neutralizing
326 mAbs and their recognized epitopes is therefore the first crucial step for
327 understanding the protective antibody response, which can inform the rational
328 development of antibody-based therapy and vaccines(*17, 18*). In some
329 EBV-infected individuals, high levels of serum neutralizing antibodies have
330 been identified capable of blocking infection of both B cells and epithelia
331 cells(*9*). This finding indicates that the human immune system is able to
332 generate potent neutralizing antibodies to clear the infection and/or attenuate
333 disease progression. However, the antigen and epitope specificity, as well as
334 the potential mechanism of neutralization of these antibodies are not entirely

clear.

We report here the isolation and characterization of the human neutralizing antibody 1D8, which protects EBV infection in both B cells and epithelial cells. Passive delivery of 1D8 significantly reduced the viral loads and tumor burden of EBV-induced lymphoma in humanized mice. Structural analysis of the 1D8-gH/gL complex identified a key epitope at the top groove of gH/gL between D-I and D-II, especially the D-II of gH, which is distinct from any of the reported antibodies. In addition, 1D8 was found to inhibit viral membrane fusion and reduce the binding of gH/gL to the epithelial cell receptor EphA2(*39, 40*). We believe that the new vulnerable site recognized by 1D8 represents another attractive target for the rational design of vaccines capable of eliciting 1D8-like neutralizing antibodies. 1D8 could also serve as a promising candidate for antibody-based therapy and prevention of EBV infection.

A couple of points need to be highlighted here. First, as both B cells and epithelia cells are major targets for EBV infection(*54*), it is highly desirable to isolate neutralizing antibodies capable of blocking the virus and protecting both cell types from infection. 1D8, together with recently reported AMMO1(*22*), are the only two representatives of this class of antibodies with dual tropism. However, we are uncertain how much this type of antibodies contributes to the overall neutralizing activities in the infected individuals. Given the low frequency in identifying 1D8 and AMMO1 antibodies among the isolated memory B cells(*22*), it is reasonable to assume they are quite rare and might

only be induced among a small proportion of naturally infected patients. Perhaps, this is due to the elusive nature of their epitopes, which are only transiently exposed during viral entry. It could also be due to their highly dynamic nature involving multiple conformational changes during infection. The rapid movement across the D-I and D-II groove required for binding and triggering of gB glycoprotein supports this notion(*30, 31, 55, 56*). Furthermore, compared to gp350, gH/gL is much less abundant and therefore has a quantitative disadvantage in immune recognition and stimulation(*19*). However, identification of 1D8 and AMMO1 and their epitopes around D-I and D-II offer an unprecedented opportunity to expose this vulnerable site in much more precise and persistent manner so that more focused and stronger immune response like 1D8 and AMMO1 could be generated. This could be done either by including gH/gL in the vaccine regimen(*9, 23*) or singling out D-I and D-II domain as epitope-focused immunogens. Both approaches would require careful design and validation to ensure proper structure and exposure of vulnerable sites recognized by 1D8 and AMMO1. In support of this notion, nanoparticles displaying gH/gL elicited a strong neutralizing antibody response against EBV infection of both target cell types(*9*), even if this exciting report requires further confirmation. Lastly, given the relatively conserved nature of this region among herpesviruses(*24, 27*), carefully designed D-I and D-II immunogens may be able to induce an even broader and stronger cross-neutralizing antibody response against a wide variety of viral strains.

379 Second, despite structural and functional insights, we are still not certain of
380 the exact mechanism through which 1D8 neutralizes EBV infection of both
381 target cell types. Structurally, 1D8 recognized a key epitope within the groove
382 between D-I and D-II, especially the D-II of gH, whereas AMMO1 was found to
383 bind a discontinuous epitope spanning D-I and D-II on the opposite ridge of the
384 groove(*22*). Such convergence on D-I and D-II domains suggests a common
385 mechanism of neutralization, either by affecting coordination within and across
386 D-I and D-II or their interaction with other viral glycoproteins such as gB or
387 gp42 required for downstream viral entry (Fig. 6A,B). AMMO1 was postulated
388 to lock D-I, D-II and the linker helix, preventing proper movement required for
389 interaction and activation of gB(*56*). As residues with the D-I and D-II groove
390 also mediate membrane fusion and several of these critical residues are near
391 the epitope of 1D8(*30, 31, 55, 56*), it stands to reason that 1D8 could also exert
392 its neutralization activity by inhibiting the fusion process. Instead of acting like
393 a molecular clamp as AMMO1, 1D8 may act more like a molecular wedge
394 forcing into the space within the groove. Certainly, as 1D8 and AMMO1 bind
395 distinct epitopes, there must be some differences in the exact mechanisms
396 underlying their inhibitory effects. For example, AMMO1 appears to be more
397 potent than 1D8 in interfering with the binding of gH/gL to B cells (Fig. 5E),
398 perhaps due to its ability to displace the c-terminal domain of gp42 through the
399 gp42 N173 glycan(*22*). Conversely, 1D8 seems to be more powerful than
400 AMMO1 in inhibiting binding of gH/gL to epithelia cells, likely by affecting the

interaction between EphA2-Fc and gH/gL (Fig. 5F,G and 6A). In any case, the 1D8 antibody identified in this study represents another potent human neutralizing antibody that can be used alone or in combination with other antibodies such as AMMO1 for antibody-based interventions against EBV infection. The epitope defined here will also assist the rational design of vaccines focusing more on the vulnerable sites to elicit powerful neutralizing antibodies similar to 1D8 and AMMO1.

MATERIALS AND METHODS

Human subjects

We collected plasma samples from 48 participants including 23 histologically diagnosed NPC cases and 25 non-NPC high-risk healthy controls in a screening program in Sihui County in Guangdong Province of China from 2007 and 2018. Peripheral blood mononuclear cell (PBMC) sample of donors 27 were collected in 2018. The screening program has been introduced in detail in other manuscript. This study was reviewed and approved by the Ethics Committee of the Sun Yat-Sen University Cancer Center (SYSUCC; Guangzhou, Guangdong, China) and was conducted in accordance with the Declaration of Helsinki.

Cell lines

All cell lines were cultured at 37℃ in a humidified atmosphere comprising 5%

CO_2. 293T cells (ATCC) were grown in DMEM (GIBCO) +10% FBS (GIBCO). CHO K-1 cells (ATCC) were maintained in Ham's F-12 (GIBCO) +10% FBS. Raji cells (ATCC), HNE1 cells(*57*) and HK1 cells(*58*) were maintained in RMPI1640+10% FBS. Akata B cells(*59*) harboring a modified EBV, in which the thymidine kinase gene has been replaced with a neomycin and green fluorescence protein (GFP) cassette (Akata-GFP), were grown in RMPI 1640 (GIBCO) +5% FBS. 293F cells (ThermoFisher) were maintained in Freestyle 293 medium (Union) with gentle shaking. All cells were grown with 100U/ml pencillin and 100μg/ml streptomycin.

Humanized mice

The construction of the humanized mice was based on NOD.*Cg-Prkdc*^{em1IDMO}*Il2rg*^{em2IDMO} mice (NOD-*Prkdc*^{null} *IL2R*γ^{null}, NPI®)(*60*), which were kept in a specific pathogen free (SPF) facility and obtained from BEIJING IDMO Co., Ltd. To generate the humanized immune system, mice were i.p. injected with a single dose of Busulfan at 20mg/kg body weight. After 48h post-injection, the mice received an intravenous tail injection of human CD34+ cells, which were isolated from umbilical cord blood (Beijing Novay biotech) with a purity of over 90%. Human CD45+ cells in peripheral blood of each humanized mouse were detected at 4 and 8 weeks post engraftment by flow cytometry.

Plasmids

The gH/gL [residues 19 to 679 of gH and residues 24 to 137 of gL were linked by $(G4S)_3$] and gp42 (residue 34 to 223) fragments were amplified from the bacterial artificial chromosome (BAC) of EBV-M81 by PCR and cloned into the pcDNA3.1 plasmid with an N-terminal CD5 leader peptide and a C-terminal HIS Tag. Targeted mutations were introduced into pcDNA3.1-CD5-gH/gL using the ClonExpress MultiS One Step Cloning Kit (Vazyme) and were confirmed by Sanger sequencing. The pCAGGS expression plasmids for gH, gL, gB, and pT7EMCLuc (which carries a luciferase-containing reporter plasmid under the control of the T7 promoter) were kindly provided by Dr. R. Longnecker. The ectodomain of EphA2 was cloned in an Fc construct as described previously(*61*).

Recombinant antibody cloning

The VH and VK/Vλ genes of reference antibodies CL40, E1D1 and AMMO1 were obtained from PDB and codon optimized genes were synthesized by Tsingke Biological Technology Company. Antibody heavy chain and light chain variable gene fragments were obtained using separate primer pairs(*62*) with restriction enzyme cutting sites, including VH primers with 5'AgeI and 3'SalI, VK primers with 5'AgeI and 3'BsiWI, and Vλ primers with 5'AgeI and 3'XhoI. Then PCR products were cloned into antibody expression vectors containing the constant regions of human IgG1. The sequences of the recombinant

plasmids were verified by Sanger sequencing.

Recombinant protein expression

The 293F cells were transfected with plasmids encoding EBV glycoproteins, EphA2-Fc and recombinant antibodies at a density of 1.5×10^6 cells/ml in Freestyle 293 medium using PEI (Polysciences) transfection reagent according to the manufacturer's instructions. After five days, the culture supernatant containing EBV glycoprotein was collected and passed through Ni-NTA resin (GE Healthcare), followed by washing (PBS with 20mM imidazole, pH7.4) and elution (PBS with 250mM imidazole, pH7.4). The proteins were further purified by size exclusion chromatography (SEC) and dialyzed into PBS. Clarified cell supernatant containing recombinant antibodies or EphA2-Fc was passed over Protein A agarose (GenScript), followed by extensive washing with PBS, and then eluted with 10 mL of 0.3M glycine, pH 2.0 into 1 mL of 1M Tris HCl, pH 8.0. Purified proteins were then dialyzed into PBS.

Recombinant protein biotinylation

gH/gL were biotinylated at a theoretical 1.5:1 biotin/protein ratio using the EZ-Link Sulfo-NHS-Biotin (ThermoFisher) at room temperature for 30min. Free biotin was removed by 3 successive rounds of dilution with PBS.

Preparation of the antigen binding fragment

1D8 Fab was obtained by digesting 1D8 IgG with Endoproteinase Lys-C (Sigma) at 37℃(1 mg IgG: 250 ng Lys C) for 12h. Fab fragments were isolated with Fc fragments using protein A agarose, then further purified by SEC.

Biolayer Interferometry (BLI)

Antibody competition binding assays (Octet Red 96, ForteBio, Pall LLC): 250nM gH/gL was captured onto HIS1K sensors (ForteBio, Pall LLC) for 120s. The baseline interference was then read for 60 s in KB buffer (PBS, 0.1% BSA, 0.02%Tween). Then the sensor was loaded with 1D8 (10μg/ml) or KB (blank) for 60s and balanced in KB for 60s, followed by association with 10μg/ml competitive antibodies (1D8, AMMO1, CL40, E1D1) for 120s and association with KB for 120s. One gH/gL-1D8 loaded sensor was immersed in buffer as a reference during the association and dissociation steps and used to subtract the background signal.

Antibody/EphA2 competition binding assays: 2μg/ml gH/gL-biotin was immobilized on streptavidin biosensors (ForteBio, Pall LLC), and then immersed into KB for 60s. Then the sensor was loaded with 1D8 (50nM), AMMO1 (50nM), 2G4 (50nM) or KB (blank) for 60s and balanced in KB for 60s, followed by associated with 1000nM EphA2-Fc for 100s and association with KB for 120s. One gH/gL-antibody loaded sensor was immersed in buffer as a reference during the association and dissociation steps and used to subtract the background signal.

Surface Plasmon Resonance (SPR)

The binding kinetics and affinity of antibodies for gH/gL or their mutants were analyzed by SPR (Biacore 8K, GE Healthcare). Anti-human IgG (Fc) antibody was covalently immobilized onto a CM5 sensor chip (GE Healthcare) via amine groups in 10 mM sodium acetate buffer (pH 5.0) for a final RU of around 5000. Specifically, antibodies 1D8 or AMMO1 (2μg/ml) were captured by anti-human IgG antibody for 10s. Diluted gH/gL or their mutants were run at a flow rate of 30 μl/min in HBS-EP (aqueous buffer containing 0.01M HEPES pH7.4, 0.15M NaCl, 3mM EDTA and 0.05%(v/v) Tween 20, filtered through a 0.2μm filter). The sensograms were fit to a 1:1 binding model using the Biacore Insight Evaluation Software (GE Healthcare).

Enzyme-Linked Immunosorbent Assay (ELISA)

For ELISA, 100ng/well of EBV glycoprotein was coated in 96-well enzyme-linked immunosorbent assay plates overnight at 4℃. Then, the plates were blocked with 5% bovine serum albumin (BSA) in PBS and 0.1%Tween-20 (blocking buffer) at 37℃ for 1 h. After blocking, the plates were washed three times with 0.1% Tween-20 in PBS (washing buffer). Plasma samples or recombinant antibodies were diluted serially in blocking buffer and incubated at 37℃ for 1 h. Following three times of washing, a 1:4000 goat anti-human IgG-HRP (Promega) in blocking buffer was added to each well and incubated

533 at 37℃ for 45 minutes. Plates were washed five times and incubated with
534 3,3',5,5'-tetramethylbenzidine substrate (TMB) (TIANGEN) for 5 minutes at
535 room temperature. Then 1M hydrochloric acid (HCl) was added and the OD_{450}
536 was read on a microplate reader (Epoch2). For the binding analysis of gH/gL
537 mutants, 500ng/well of antibody was coated in plates overnight at 4℃. The
538 plates were then blocked and washed. The gH/gL mutants were diluted serially
539 in blocking buffer and incubated at 37℃ for 1h. Following three times of
540 washing, 1:3000 diluted mouse anti-his antibody (TRANSGEN BIOTECH) in
541 blocking buffer was added to each well and incubated at 37℃ for 1h. After
542 three times of washing, a 1:5000 diluted goat anti-mouse-HRP antibody
543 (Invitrogen) was added and incubated at 37℃ for 1h. The final steps were the
544 same as above.
545
546 **B cells sorting**
547 Cryopreserved 10 million PBMC were thawed into 1 ml preheated RPMI1640,
548 centrifuged at 300×g for 5 min, re-suspended in 500μl FACS buffer (PBS+2%
549 FBS), and incubated with 200nM his-tagged antigen (gH/gL) for 45 min at 4℃.
550 The PBMC were then washed two times with 1ml FACS buffer and
551 resuspended in 100μl FACS buffer. The PBMC were stained with the following
552 antibodies: CD3-PE-Cy5 (BD Biosciences) at a 1:25 dilution, CD14-PE-Cy5
553 (eBioscience) at a 1:50 dilution, CD16-PE-Cy5 (BD Biosciences) at a 1:25
554 dilution, CD235a-PE-Cy5 (BD Biosciences) at a 1:100 dilution,

CD19-APC-Cy7 (BD Biosciences) at a 1:100 dilution, CD20-PE-Cy7 (BD Biosciences) at a 1:200 dilution, IgG-FITC (BD Biosciences) at a 1:25 dilution, and anti-his-PE (BioLegend) at a 1:20 dilution for 30 min at 4℃. The PBMC were washed three times with 1ml FACS buffer and resuspended in 500μl FACS buffer, then subjected to FACS on a BD FACS Aria II (BD Biosciences). Antigen-positive B cells (CD3-, CD14-, CD16-, CD235a-, CD19+, CD20+, IgG+, PE+) were sorted individually into 96-well PCR vital-plates containing 20μl first strand buffer (5μl first strand buffer, 0.5μl of RNase inhibitor (Invitrogen), 1.25μl of 100μM DTT, 0.06μl of IGEPAL (Sigma).

VH/VL recovery from sorted cells

Wells containing sorted cells were mixed with 6μl of reverse transcription (RT) buffer containing 1.5μl mixed primers specific for human IgG, IgM, IgD, IgA1, IgA2, K and λ constant gene regions, 1.5μl of 25 mM dNTP mix (Invitrogen), and 0.25μl of superscript III reverse transcriptase (Invitrogen). The RT temperature program included 42℃ for 10 min, 25℃ for 10 min, 60℃ for 50 min, and 94℃ for 5 min, followed by a hold at 4℃. The VH, VK and Vλ genes were amplified from 5μl of cDNA separately using nested PCR (HotStarTaq DNA Polymerase, QIAGEN). The PCR products were purified and subjected to Sanger sequencing. Then, the VH, VK and Vλ variable genes were assembled into functional linear Ig gene expression cassettes by overlap-extension PCR. The function of the expressed antibodies was determined using ELISA

screening.

Virus production

Akata cells carrying EBV, in which the thymidine kinase gene was interrupted with a double cassette expressing GFP and a neomycin resistance gene, were resuspended in FBS-free RPMI 1640 medium at a concentration of $2–3\times10^6$ cells per ml, followed by induction with 0.75% (v/v) of goat anti-human immunoglobulin G serum (Shuangliu Zhenglong Biochem Lab) for 6h at 37℃. After culture in fresh RPMI1640 medium supplemented with 5% FBS for 3 days, virus from the supernatant was collected under sterile conditions, passed through two Millipore filters (0.8 and 0.45μm), concentrated 100-fold by high-speed centrifugation at 50,000g, and then resuspended in fresh FBS-free RPMI1640. The virus was stored at 80℃ and thawed immediately before infection. To assess the virus titer, 10-fold dilutions of EBV were used to inoculate 2×10^5 PBMC per well in 24-well plates with 2μg/ml cyclosporin A (CsA) (Sigma). The cultures were fed weekly by replacing half of the medium with fresh medium containing CsA. After 6 weeks, the TD_{50} was determined based on the number of proliferating lymphocytes in the wells (*63*).

Neutralization assay

Plasma samples from study individuals or recombinant antibodies were incubated with GFP-expressing EBV at serial dilutions for 3h at 4℃. Then the

mixtures were added to Raji B cells or HNE1 epithelial cells and incubated for 3h at 37℃. Then the unbound virus was removed by washing with PBS twice. Infected cells were cultured in fresh medium for 48h, followed by detection and analysis of GFP-positive cells using a flow cytometer and FlowJo 10 software (FlowJo, USA). The neutralization rate of each sample was defined as: (%GFP+ cells in the positive control well containing virus alone - %GFP+ cells in the plasma or antibody containing well)/ %GFP+ cells in the positive control well×100.

EBV infection in humanized mice

At 8 weeks post CD34+ stem cells transfer, 0.4 mg of experimental or control antibodies were i.p. injected per humanized mouse. After 24 h, the mice received a dose of Akata EBV equivalent to 1,000 TD_{50} via i.v. injection. In the following period, the mice received a dose of 0.4mg antibody weekly. The blood collection and recording of body weight and health status were also done every week. The mice were euthanized 6 weeks post EBV infection or earlier if they became clinically ill (e.g. body weight loss of approximately 20%).

Detection of EBV DNA in blood and tissues

DNA was extracted from the peripheral blood (100μl) or tissues of the mice using commercial DNA extraction kits (Omega). The EBV genome copy

number was determined by real-time PCR (Roche Light Cycler 480) using the TaqMan BamHI probes (*40*) as described previously. The copy numbers of EBV were quantified using a standard EBV genome (BDS biotech) as control.

H&E staining, IHC, and in situ hybridization

Tissues were fixed in 10% formalin and embedded in paraffin. Consecutive sections were used for staining with H&E. Immunostaining of human T cells and B cells was performed using hCD3 antibody (VENTANA) and hCD20 antibody (VENTANA) at 1:200 dilution. EBERs were stained by in situ hybridization using the EBER detection kit (ZSGB-BIO), according to the manufacturer's instructions. Histological staining was evaluated by experienced pathologists.

Detection of human immune cells in the blood of humanized mice

Peripheral blood of mice was treated with 1ml red blood cell lysis buffer (BioLegend) at room temperature for 10min. Then the cells were centrifuged at 300×g, washed twice with PBS, re-suspended in PBS, and stained with antibodies including anti-human CD45-PE (BD Biosciences), CD3-PerCP-Cy5.5 (BD Biosciences) and CD20-FITC (BD Biosciences) at 1:100 dilution for 30 min at 4℃. After washing with PBS, the percentage of CD3+ or CD20+ cells among the CD45+ cells was quantified using a flow cytometer.

643

644 **Cell surface binding assays**

645 For the cell-surface binding assay, 1mg of gH/gL-biotin conjugated with SA-PE
646 (gH/gL-PE) was diluted in 10ml of PBS into individual wells of a 96 well plate.
647 An equimolar amount of gp42 was added to select wells containing gH/gL-PE.
648 5mg/ml of monoclonal antibodies, including 1D8, AMMO1, or 2G4, were added
649 to select wells containing gH/gL with or without gp42 and incubated for 1h at
650 37℃. At the same time, adherent HK1 cells were trypsinized (NCM Biotech),
651 washed with RMPI 1640 and then allowed to recover at 37℃ in a humidified
652 atmosphere comprising 5% CO_2 for 1h with gentle agitation twice during the
653 period. Recovered HK1 and Raji cells were pelleted by centrifugation at 300×
654 g for 5min and then resuspended at a density of $2x10^6$ cells/ml in ice-cold 0.5%
655 bovine serum albumin (BSA) in PBS. Then, 100μl of the HK1 or Raji cells
656 suspension were added to wells containing SA-PE, gH/gL-PE with or without
657 gp42 and antibodies, and incubated on ice for 1h. The cells were pelleted by
658 centrifugation at 300×g for 5min, washed with 1 ml of ice cold 0.5% BSA in
659 PBS, pelleted again and resuspended in 10% phosphate buffered formalin.
660 The amount of PE staining was quantified using a flow cytometer.

661

662 **Virus-free fusion assay**

663 Effector CHO-K1 cells were transiently transfected with expression plasmid
664 (pCAGGS-gH, pCAGGS-gL, pCAGGS-gB and pT7EMCLuc, which carries a

665 luciferase-containing reporter plasmid under the control of the T7 promoter).
666 Target cells (HEK-293T) were transfected with expression plasmid pCAGT7
667 (expressing T7 DNA polymerase). After 24h, the effector cells were trypsinized
668 and re-suspended at a density of 1×10^6 cells/ml. Aliquots comprising
669 250μl/well of effector cell suspension was pre-incubated with 2μg 1D8,
670 AMMO1 or 2G4 antibody at 37℃ for 1h. Then the target cells were also
671 trypsinized and re-suspended at a density of 1×10^6 cells/ml. An aliquot
672 comprising 250μl of the effector cell suspension was added to the effector cells
673 with or without antibody. After 24h, the medium was aspirated and the cells
674 were lysed in 100μl of luciferase agent (Dual-Glo Luciferase Assay System).
675 Then, 75μl of cell lysate was transferred to a white-bottom assay plate and
676 luciferase activity was read on a GloMax-96 Microplate Luminometer
677 (Promega).
678
679 **Cell surface staining**
680 Following 24h after expression plasmid transfection, the effector CHO-K1 cells
681 were trypsinized and re-suspended at a density of 1×10^6 cells/ml. The
682 expression level of gH/gL was detected using the indicated antibody. AMMO1
683 and 1D8 were used for gH/gL staining and 2G4 as a control. Then, 10μg/ml of
684 antibody was added to the cell suspension and incubated at 4℃ for 1h. The
685 cells were washed twice with PBS and stained with human IgG-PerCP-Cy5.5
686 (PC5.5) (BioLegend) at a 1:100 dilution. After washing with PBS, the

687 percentage of PC5.5+ cells was quantified using a flow cytometer (CytoFLEX,
688 BECKMAN).
689
690 **Crystallization of the 1D8 Fab and data collection**
691 To purify the gH/gL-1D8 Fab complex, 1D8 Fab was incubated with gH/gL for 1
692 h on ice in HBS buffer, and the mixture was then subjected to gel filtration
693 chromatography. Fractions containing the complex were pooled and
694 concentrated to 10 mg/ml. Crystals were successfully grown at 18℃ in sitting
695 drops, over wells containing 200 mM sodium citrate, 100 mM HEPES sodium
696 salt, pH 7.5, 15 % w/v MPD. The drops were made by mixing 200 nl
697 gH/gL-1D8 Fab complex in HBS buffer with 200 nl well solution. Crystals were
698 harvested, soaked briefly in 200 mM sodium citrate, 100 mM HEPES sodium
699 salt, pH 7.5, 15 % w/v MPD, 20% glycerol, and flash-frozen in liquid nitrogen.
700 Diffraction data were collected at the BL17U beam line of the Shanghai
701 Synchrotron Research Facility (SSRF). Diffraction data were processed with
702 HKL2000 and the crystal diffracted to 4.2Å. The data processing statistics are
703 listed in Supplementary Table 3.
704
705 **Structure solution and refinement**
706 The structure was determined via the molecular replacement method using
707 PHASER in CCP4 suite. The search models were gH/gL (PDB code 5T1D)
708 and the antibody with the highest sequence identity with 1D8. Density map

improvement by atoms update and refinement was performed with ARP/wARP29. Subsequent model building and refinement were performed using COOT and PHENIX, respectively. Final Ramachandran statistics indicated that 91.48% residues were in favored conformations, 7.06% allowed and 1.46% outliers for the final structure. The structural refinement statistics are listed in Supplementary Table 3. All structural figures were generated with PyMol (DeLano, 2002).

Statistical analysis

Unless noted otherwise, a two-tailed, unpaired *t*-test was used to assess statistical significance. Statistical calculations were performed in GraphPad Prism 8. The number of replicates and a description of the statistical method are provided in the corresponding figure legends. Differences with P values of less than 0.05 were considered to be statistically significant. * $P < 0.05$, ** $P < 0.01$, *** $P < 0.001$, ns=not significant.

REFERENCES AND NOTES

1. G. de-The *et al.*, Sero-epidemiology of the Epstein-Barr virus: preliminary analysis of an international study - a review. *IARC Sci Publ*, 3-16 (1975).
2. L. S. Young, L. F. Yap, P. G. Murray, Epstein-Barr virus: more than 50 years old and still providing surprises. *Nat Rev Cancer* **16**, 789-802 (2016).
3. J. I. Cohen, A. S. Fauci, H. Varmus, G. J. Nabel, Epstein-Barr virus: an important vaccine target for cancer prevention. *Sci Transl Med* **3**, 107fs107 (2011).
4. L. S. Young, C. W. Dawson, Epstein-Barr virus and nasopharyngeal carcinoma. *Chin J Cancer* **33**, 581-590 (2014).
5. S. E. Henrickson, To EBV or not to EBV: Rational vaccine design for a common infection. *Sci Immunol* **3**, (2018).
6. D. G. van Zyl, J. Mautner, H. J. Delecluse, Progress in EBV Vaccines. *Front Oncol* **9**, 104 (2019).

7. J. I. Cohen, Epstein-barr virus vaccines. *Clin Transl Immunology* **4**, e32 (2015).
8. J. I. Cohen, E. S. Mocarski, N. Raab-Traub, L. Corey, G. J. Nabel, The need and challenges for development of an Epstein-Barr virus vaccine. *Vaccine* **31 Suppl 2**, B194-196 (2013).
9. W. Bu *et al.*, Immunization with Components of the Viral Fusion Apparatus Elicits Antibodies That Neutralize Epstein-Barr Virus in B Cells and Epithelial Cells. *Immunity* **50**, 1305-1316 e1306 (2019).
10. A. E. Coghill *et al.*, High Levels of Antibody that Neutralize B-cell Infection of Epstein-Barr Virus and that Bind EBV gp350 Are Associated with a Lower Risk of Nasopharyngeal Carcinoma. *Clin Cancer Res* **22**, 3451-3457 (2016).
11. A. E. Coghill *et al.*, Evaluation of Total and IgA-Specific Antibody Targeting Epstein-Barr Virus Glycoprotein 350 and Nasopharyngeal Carcinoma Risk. *J Infect Dis* **218**, 886-891 (2018).
12. W. Bu *et al.*, Kinetics of Epstein-Barr Virus (EBV) Neutralizing and Virus-Specific Antibodies after Primary Infection with EBV. *Clin Vaccine Immunol* **23**, 363-369 (2016).
13. J. Sashihara, P. D. Burbelo, B. Savoldo, T. C. Pierson, J. I. Cohen, Human antibody titers to Epstein-Barr Virus (EBV) gp350 correlate with neutralization of infectivity better than antibody titers to EBV gp42 using a rapid flow cytometry-based EBV neutralization assay. *Virology* **391**, 249-256 (2009).
14. D. Sok, D. R. Burton, Recent progress in broadly neutralizing antibodies to HIV. *Nat Immunol* **19**, 1179-1188 (2018).
15. E. O. Saphire, S. L. Schendel, B. M. Gunn, J. C. Milligan, G. Alter, Antibody-mediated protection against Ebola virus. *Nat Immunol* **19**, 1169-1178 (2018).
16. F. Yu *et al.*, Receptor-binding domain-specific human neutralizing monoclonal antibodies against SARS-CoV and SARS-CoV-2. *Signal Transduct Target Ther* **5**, 212 (2020).
17. L. M. Walker, D. R. Burton, Passive immunotherapy of viral infections: 'super-antibodies' enter the fray. *Nat Rev Immunol* **18**, 297-308 (2018).
18. A. Lanzavecchia, A. Fruhwirth, L. Perez, D. Corti, Antibody-guided vaccine design: identification of protective epitopes. *Curr Opin Immunol* **41**, 62-67 (2016).
19. L. M. Hutt-Fletcher, EBV glycoproteins: where are we now? *Future Virol* **10**, 1155-1162 (2015).
20. B. S. Mohl, J. Chen, R. Longnecker, Gammaherpesvirus entry and fusion: A tale how two human pathogenic viruses enter their host cells. *Adv Virus Res* **104**, 313-343 (2019).
21. T. Haque *et al.*, A mouse monoclonal antibody against Epstein-Barr virus envelope glycoprotein 350 prevents infection both in vitro and in vivo. *J Infect Dis* **194**, 584-587 (2006).
22. J. Snijder *et al.*, An Antibody Targeting the Fusion Machinery Neutralizes Dual-Tropic Infection and Defines a Site of Vulnerability on Epstein-Barr Virus. *Immunity* **48**, 799-811 e799 (2018).
23. X. Cui *et al.*, Rabbits immunized with Epstein-Barr virus gH/gL or gB recombinant proteins elicit higher serum virus neutralizing activity than gp350. *Vaccine* **34**, 4050-4055 (2016).
24. S. A. Connolly, J. O. Jackson, T. S. Jardetzky, R. Longnecker, Fusing structure and function: a structural view of the herpesvirus entry machinery. *Nat Rev Microbiol* **9**, 369-381 (2011).
25. S. Singh *et al.*, Neutralizing Antibodies Protect against Oral Transmission of Lymphocryptovirus. *Cell Rep Med* **1**, (2020).
26. B. S. Mohl, J. Chen, K. Sathiyamoorthy, T. S. Jardetzky, R. Longnecker, Structural and Mechanistic Insights into the Tropism of Epstein-Barr Virus. *Mol Cells* **39**, 286-291 (2016).
27. S. A. Connolly, T. S. Jardetzky, R. Longnecker, The structural basis of herpesvirus entry. *Nat Rev Microbiol*, (2020).

28. L. S. Chesnokova, L. M. Hutt-Fletcher, Epstein-Barr virus infection mechanisms. *Chin J Cancer* **33**, 545-548 (2014).
29. H. Matsuura, A. N. Kirschner, R. Longnecker, T. S. Jardetzky, Crystal structure of the Epstein-Barr virus (EBV) glycoprotein H/glycoprotein L (gH/gL) complex. *Proc Natl Acad Sci U S A* **107**, 22641-22646 (2010).
30. B. S. Mohl, K. Sathiyamoorthy, T. S. Jardetzky, R. Longnecker, The conserved disulfide bond within domain II of Epstein-Barr virus gH has divergent roles in membrane fusion with epithelial cells and B cells. *J Virol* **88**, 13570-13579 (2014).
31. J. Chen, T. S. Jardetzky, R. Longnecker, The large groove found in the gH/gL structure is an important functional domain for Epstein-Barr virus fusion. *J Virol* **87**, 3620-3627 (2013).
32. K. Sathiyamoorthy *et al.*, Assembly and architecture of the EBV B cell entry triggering complex. *PLoS Pathog* **10**, e1004309 (2014).
33. M. Kanekiyo *et al.*, Rational Design of an Epstein-Barr Virus Vaccine Targeting the Receptor-Binding Site. *Cell* **162**, 1090-1100 (2015).
34. K. A. Young, A. P. Herbert, P. N. Barlow, V. M. Holers, J. P. Hannan, Molecular basis of the interaction between complement receptor type 2 (CR2/CD21) and Epstein-Barr virus glycoprotein gp350. *J Virol* **82**, 11217-11227 (2008).
35. G. Szakonyi *et al.*, Structure of the Epstein-Barr virus major envelope glycoprotein. *Nat Struct Mol Biol* **13**, 996-1001 (2006).
36. K. Sathiyamoorthy *et al.*, Structural basis for Epstein-Barr virus host cell tropism mediated by gp42 and gHgL entry glycoproteins. *Nat Commun* **7**, 13557 (2016).
37. M. M. Mullen, K. M. Haan, R. Longnecker, T. S. Jardetzky, Structure of the Epstein-Barr virus gp42 protein bound to the MHC class II receptor HLA-DR1. *Mol Cell* **9**, 375-385 (2002).
38. A. N. Kirschner, J. Omerovic, B. Popov, R. Longnecker, T. S. Jardetzky, Soluble Epstein-Barr virus glycoproteins gH, gL, and gp42 form a 1:1:1 stable complex that acts like soluble gp42 in B-cell fusion but not in epithelial cell fusion. *J Virol* **80**, 9444-9454 (2006).
39. J. Chen *et al.*, Ephrin receptor A2 is a functional entry receptor for Epstein-Barr virus. *Nat Microbiol* **3**, 172-180 (2018).
40. H. Zhang *et al.*, Ephrin receptor A2 is an epithelial cell receptor for Epstein-Barr virus entry. *Nat Microbiol* **3**, 1-8 (2018).
41. H. B. Wang *et al.*, Neuropilin 1 is an entry factor that promotes EBV infection of nasopharyngeal epithelial cells. *Nat Commun* **6**, 6240 (2015).
42. J. Chen, R. Longnecker, Epithelial cell infection by Epstein-Barr virus. *FEMS Microbiol Rev* **43**, 674-683 (2019).
43. K. Sathiyamoorthy *et al.*, Inhibition of EBV-mediated membrane fusion by anti-gHgL antibodies. *Proc Natl Acad Sci U S A* **114**, E8703-E8710 (2017).
44. Z. Liu *et al.*, Two Epstein-Barr virus-related serologic antibody tests in nasopharyngeal carcinoma screening: results from the initial phase of a cluster randomized controlled trial in Southern China. *Am J Epidemiol* **177**, 242-250 (2013).
45. Y. Liu *et al.*, Establishment of VCA and EBNA1 IgA-based combination by enzyme-linked immunosorbent assay as preferred screening method for nasopharyngeal carcinoma: a two-stage design with a preliminary performance study and a mass screening in southern China. *Int J Cancer* **131**, 406-416 (2012).
46. S. Fujiwara, K. Imadome, M. Takei, Modeling EBV infection and pathogenesis in

new-generation humanized mice. *Exp Mol Med* **47**, e135 (2015).
47. E. K. Lee *et al.*, Effects of lymphocyte profile on development of EBV-induced lymphoma subtypes in humanized mice. *Proc Natl Acad Sci U S A* **112**, 13081-13086 (2015).
48. C. Munz, Humanized mouse models for Epstein Barr virus infection. *Curr Opin Virol* **25**, 113-118 (2017).
49. E. A. Caves *et al.*, Air-Liquid Interface Method To Study Epstein-Barr Virus Pathogenesis in Nasopharyngeal Epithelial Cells. *mSphere* **3**, (2018).
50. R. Lin *et al.*, Development of a robust, higher throughput green fluorescent protein (GFP)-based Epstein-Barr Virus (EBV) micro-neutralization assay. *J Virol Methods* **247**, 15-21 (2017).
51. D. R. Burton, L. Hangartner, Broadly Neutralizing Antibodies to HIV and Their Role in Vaccine Design. *Annu Rev Immunol* **34**, 635-659 (2016).
52. L. L. Lu, T. J. Suscovich, S. M. Fortune, G. Alter, Beyond binding: antibody effector functions in infectious diseases. *Nat Rev Immunol* **18**, 46-61 (2018).
53. G. Zhou, Q. Zhao, Perspectives on therapeutic neutralizing antibodies against the Novel Coronavirus SARS-CoV-2. *Int J Biol Sci* **16**, 1718-1723 (2020).
54. O. A. Odumade, K. A. Hogquist, H. H. Balfour, Jr., Progress and problems in understanding and managing primary Epstein-Barr virus infections. *Clin Microbiol Rev* **24**, 193-209 (2011).
55. B. S. Mohl, J. Chen, S. J. Park, T. S. Jardetzky, R. Longnecker, Epstein-Barr Virus Fusion with Epithelial Cells Triggered by gB Is Restricted by a gL Glycosylation Site. *J Virol* **91**, (2017).
56. J. Omerovic, L. Lev, R. Longnecker, The amino terminus of Epstein-Barr virus glycoprotein gH is important for fusion with epithelial and B cells. *J Virol* **79**, 12408-12415 (2005).
57. F. Zhan *et al.*, [Primary study of differentially expressed cDNA sequences in cell line HNE1 of human nasopharyngeal carcinoma by cDNA representational difference analysis]. *Zhonghua Yi Xue Yi Chuan Xue Za Zhi* **15**, 341-344 (1998).
58. D. P. Huang *et al.*, Establishment of a cell line (NPC/HK1) from a differentiated squamous carcinoma of the nasopharynx. *Int J Cancer* **26**, 127-132 (1980).
59. S. J. Molesworth, C. M. Lake, C. M. Borza, S. M. Turk, L. M. Hutt-Fletcher, Epstein-Barr virus gH is essential for penetration of B cells but also plays a role in attachment of virus to epithelial cells. *J Virol* **74**, 6324-6332 (2000).
60. S. Guo *et al.*, Oncological and genetic factors impacting PDX model construction with NSG mice in pancreatic cancer. *FASEB J* **33**, 873-884 (2019).
61. J. Chen, S. Schaller, T. S. Jardetzky, R. Longnecker, EBV gH/gL and KSHV gH/gL bind to different sites on EphA2 to trigger fusion. *J Virol*, (2020).
62. H. X. Liao *et al.*, High-throughput isolation of immunoglobulin genes from single human B cells and expression as monoclonal antibodies. *J Virol Methods* **158**, 171-179 (2009).
63. M. Yajima *et al.*, A new humanized mouse model of Epstein-Barr virus infection that reproduces persistent infection, lymphoproliferative disorder, and cell-mediated and humoral immune responses. *J Infect Dis* **198**, 673-682 (2008).

Acknowledgements: We thank Chang Song and Cui Qiao from Beijing IDMO Company for help with the animal experiment. The plasmids pCAGGS-T7,

pCAGGS-gH, pCAGGS-gL, pCAGGS-gB and pT7EMCLuc were kindly provided by Professor Richard Longnecker. **Funding:** This work was supported by the following grant supports: the National Key Research and Development Program of China (2017YFA0505600, 2016YFA0502100, 2018ZX10731101-002, 2017ZX10201101), the National Natural Science Foundation of China (81530065, 81520108022, 81830090 and 81621004), Guangdong Province key research and development program (2019B020226002) and Beijing Municipal Science & Technology Commission (Z181100001918043, 171100000517). **Author contributions:** L.Z., M.Z., and X.W. conceptualized the study. Q.Z., S.S., J.Y., Y.Z., and C.S. performed experiments and analyzed data. Q.Z., S.S., J.Y., L.Z., M.Z., and X.W. wrote the manuscript, and all authors contributed to editing and figure preparation. Funding was secured by L.Z., M.Z., and X.W. **Competing interests**: The authors declare no potential conflicts of interest. **Data availability:** The atomic model of 1D8-gH/gL (PDB ID: 7D5Z) has been deposited in the Protein Data Bank.

MAIN FIGURE LEGENDS

Fig. 1. Isolation of gH/gL-specific monoclonal antibodies using single B cell sorting and cloning. (**A**) FACS-based sorting strategy for gH/gL-specific B cells. (**B**) Binding activities of 1D8 and 2A6, the positive control AMMO1, and the negative control 2G4 to EBV gH/gL measured by ELISA. The data are presented as means ± SEM. (**C**) Neutralizing activities of 1D8 and 2A6, the positive control AMMO1, and the negative control 2G4 against EBV infection of Raji B cell lines and (**D**) HNE1 epithelia cell line. The data shown is means ± SEM. SSC-A, side-scatter area; FSC-A, forward-scatter area.

Fig. 2. Protective efficacy of 1D8 against lethal EBV challenge in humanized mice. (**A**) Timeline for engrafting CD34+ human hematopoietic stem cells (HSC), antibody administration, viral challenge, and monitoring for various biological and clinical outcomes. Four hundred micrograms of 1D8, positive control AMMO1, negative control 2G4, or PBS negative control were administered to the humanized mice via intraperitoneal injection either 24h prior to or weekly for 5 weeks after intravenous challenge with Akata EBV. (**B**) EBV DNA in the peripheral blood, (**C**) body weight, and (**D**) survival were monitored weekly. The percent changes in (**E**) hCD45+, (**F**) hCD20+, or (**G**) hCD3+ cells over the experiment period. On week 6 post infection, (**H**) virus titers in spleen, (**I**) liver, (**J**) kidney were analyzed. All data are presented as mean ± SEM. *$p < 0.05$; **$p < 0.01$; ***$p < 0.001$; ns, no significant.

911

912 **Fig. 3. 1D8 reduces viral replication and tissue damages in humanized**
913 **mice.** Representative of macroscopic spleens and splenic sections stained for
914 hematoxylin and eosin (H&E), EBV encoded RNA (EBER), human CD20
915 (hCD20), and human CD3 (hCD3) at necropsy. The scale bars are indicated.

916

917 **Fig. 4. 1D8 targets an unique epitope on gH/gL.** (**A**) Structure overview in a
918 cartoon representation with gL in cyan, gH D-I in blue, D-II in wheat, D-III in
919 green, D-IV in yellow, and 1D8 Fab in purple. The map is contoured at 1.2
920 RMS to show the density. (**B**) Zoomed-in view of the interaction between 1D8
921 and D-I and D-II. The key binding residue N310 of gH was indicated by a red
922 star. (**C**) Cartoon representation of Fab 1D8 and other previously published
923 Fabs AMMO1, CL40, and E1D1 bound to a single gH/gL molecule. The color
924 scheme for gH/gL is as in (**A**) whereas 1D8 Fab in purple, AMMO1 Fab in light
925 blue, CL40 Fab in pink, and E1D1 Fab in dark green. (**D**) Surface mapping of
926 the four Fab epitopes on gH/gL with the same color in (**C**). Areas in black
927 indicate the region where structural change was found upon binding to
928 AMMO1 or CL40.

929

930 **Fig. 5. 1D8 interferes with cell fusion and binding.** Quality control of gH/gL
931 expression on the surface of CHO-K1 cells by staining with 1D8 (**A**), positive
932 control AMMO1 (**B**), and negative control 2G4 (**C**) before proceeded to the

933 fusion experiment shown in (**D**). (**D**) Marked reduction in cell-cell fusion in the
934 presence of 1D8, the positive control AMMMO1, but not the negative control
935 2G4. Marked reduction in gH/gL binding to Raji B cell (**E**) and HK1 epithelial
936 cell (**F**) in the presence of 1D8, the positive control AMMO1, but not the
937 negative control 2G4. Binding of EphA1-Fc to gH/gL was reduced by 1D8 (**G**),
938 but not by AMMO1 (**H**) or 2G4 (**I**) measured by Bio-layer interferometry (BLI).
939 All data are presented as mean ± SEM. *$p < 0.05$; **$p < 0.01$; ***$p < 0.001$; ns,
940 no significant. SSC-A, side-scatter area; PC5.5, PerCP-Cy5.5; RLU, relative
941 light unit; SA-PE, streptavidin-phycoerythrin; MFI, mean fluorescence intensity.
942
943 **Fig. 6. Possible mechanisms of 1D8-mediated neutralization.** (**A**) For
944 epithelia cells, 1D8 could interfere the interaction between gH/gL and EphA2
945 either by directly restricting access to the interface or by indirectly posing
946 allosteric hindrance. It could also restrict the movement across the D-I/D-II
947 groove of gH/gL that is required for gB interaction and triggering. (**B**) For B
948 cells, 1D8 could also restrict the movement across the D-I/D-II groove of gH/gL
949 that is required for downstream viral entry. 1D8 does not appear influence
950 interaction between gp42 and its receptor HLA class II.
951
952
953
954

Fig. 1

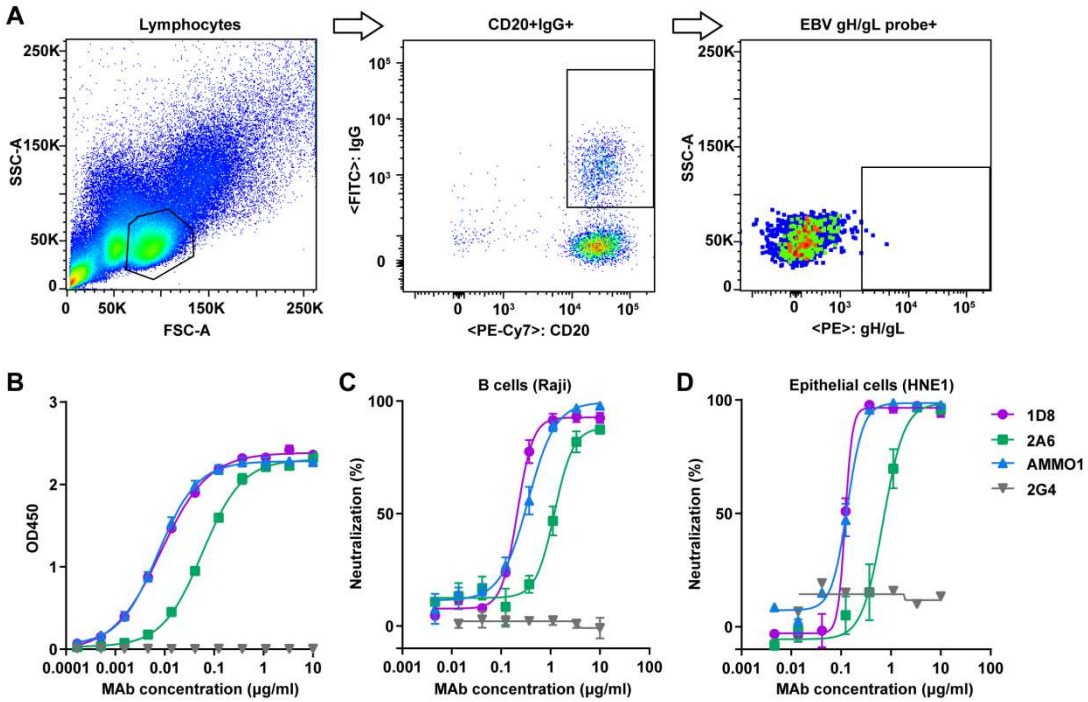
A
Lymphocytes
SSC-A
FSC-A
CD20+IgG+
<FITC>: IgG
<PE-Cy7>: CD20
EBV gH/gL probe+
<PE>: gH/gL
B
OD450
MAb concentration (μg/ml)
C
B cells (Raji)
Neutralization (%)
MAb concentration (μg/ml)
D
Epithelial cells (HNE1)
Neutralization (%)
MAb concentration (μg/ml)
1D8
2A6
AMMO1
2G4

969 **Fig. 2**

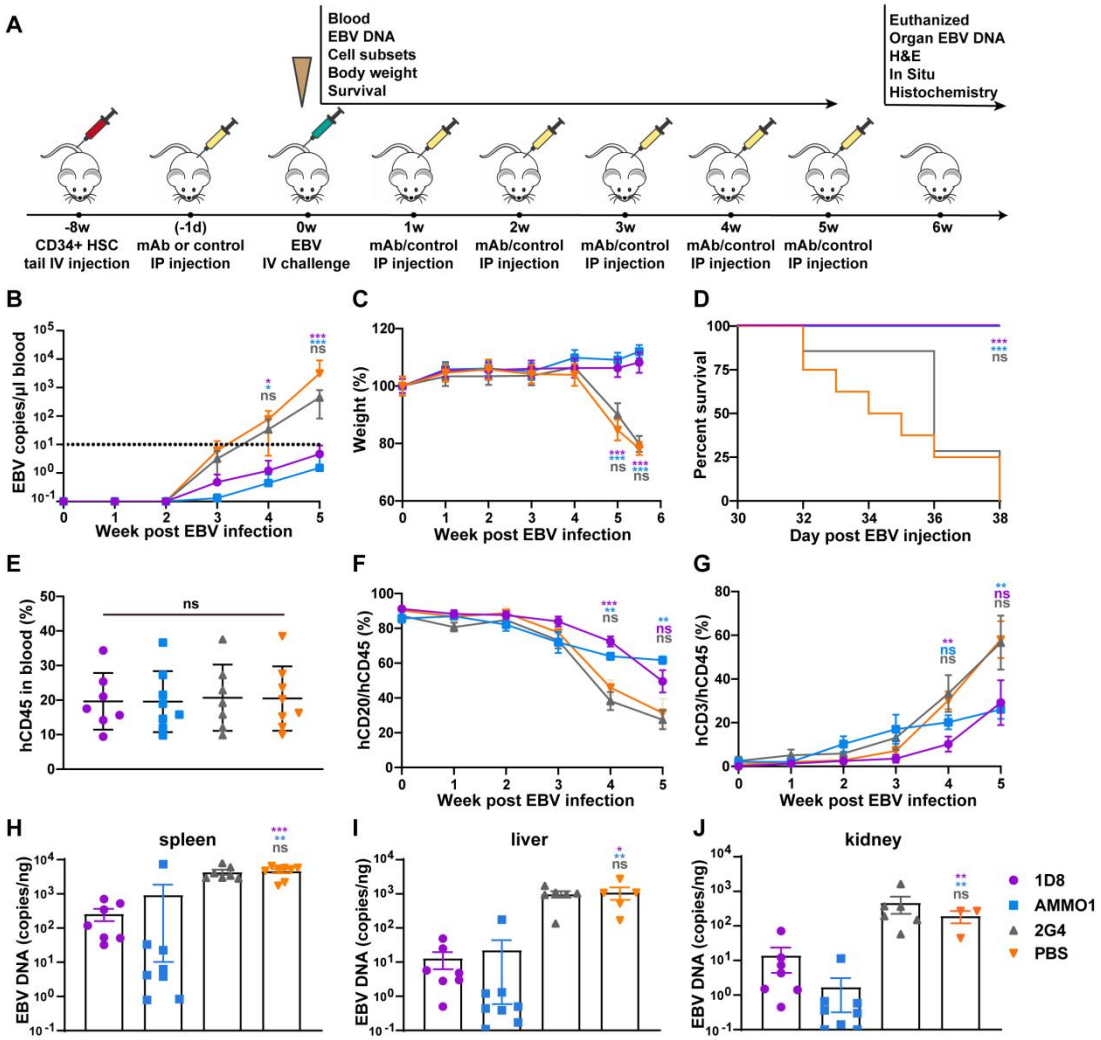

970

971

972

973

974

975

976

977

978

Fig. 3

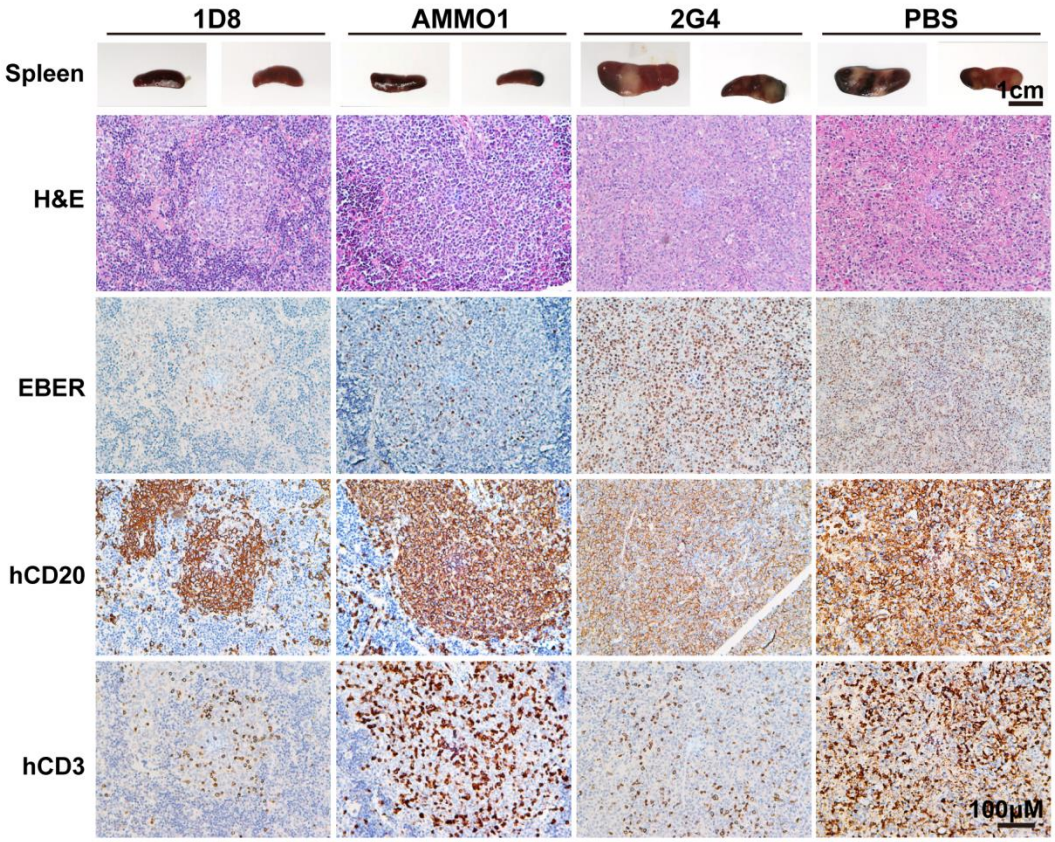

Fig. 4

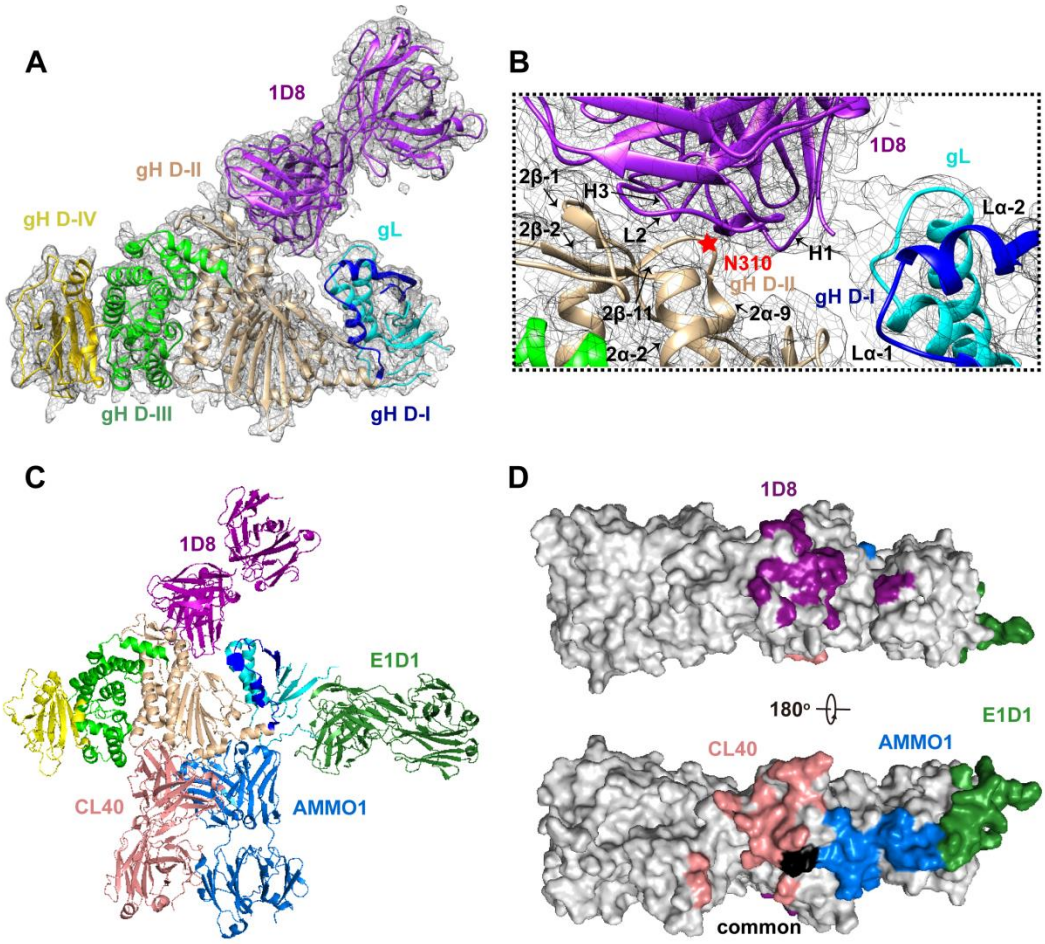
A
1D8
gH D-II
gH D-IV
gL
gH D-III
gH D-I
B
1D8
gL
2β-1
H3
Lα-2
2β-2
L2
H1
N310
gH D-II
gH D-I
2β-11
2α-9
2α-2
Lα-1
C
1D8
E1D1
CL40
AMMO1
D
1D8
180°
E1D1
CL40
AMMO1
common

Fig. 5

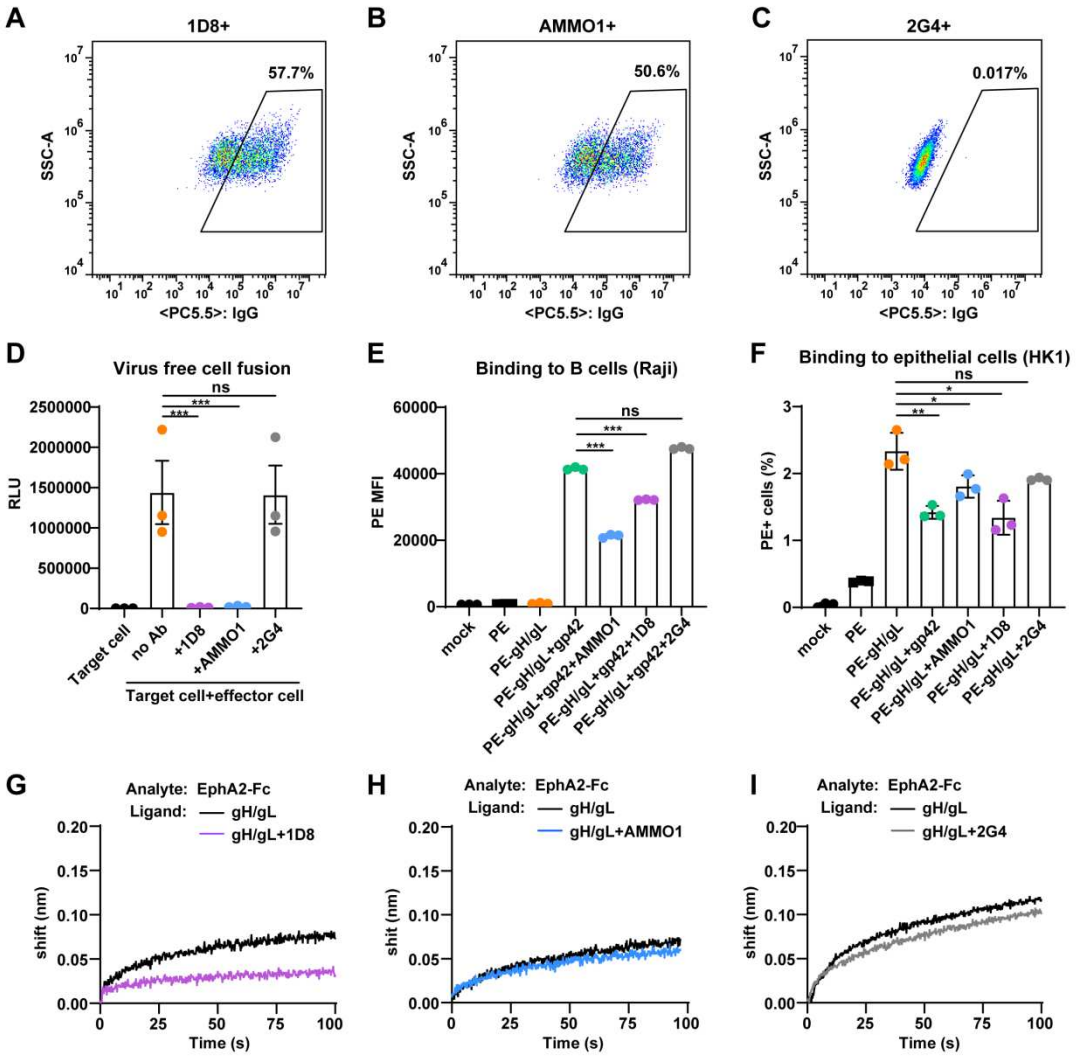
A
1D8+
57.7%
SSC-A
<PC5.5>: IgG
B
AMMO1+
50.6%
SSC-A
<PC5.5>: IgG
C
2G4+
0.017%
SSC-A
<PC5.5>: IgG
D
Virus free cell fusion
RLU
ns
***
***
Target cell
no Ab
+1D8
+AMMO1
+2G4
Target cell+effector cell
E
Binding to B cells (Raji)
PE MFI
ns
***
***
mock
PE
PE-gH/gL
PE-gH/gL+gp42
PE-gH/gL+gp42+AMMO1
PE-gH/gL+gp42+1D8
PE-gH/gL+gp42+2G4
F
Binding to epithelial cells (HK1)
PE+ cells (%)
ns
*
*
**
mock
PE
PE-gH/gL
PE-gH/gL+gp42
PE-gH/gL+AMMO1
PE-gH/gL+1D8
PE-gH/gL+2G4
G
Analyte: EphA2-Fc
Ligand: gH/gL
gH/gL+1D8
shift (nm)
Time (s)
H
Analyte: EphA2-Fc
Ligand: gH/gL
gH/gL+AMMO1
shift (nm)
Time (s)
I
Analyte: EphA2-Fc
Ligand: gH/gL
gH/gL+2G4
shift (nm)
Time (s)

1012 **Fig. 6**

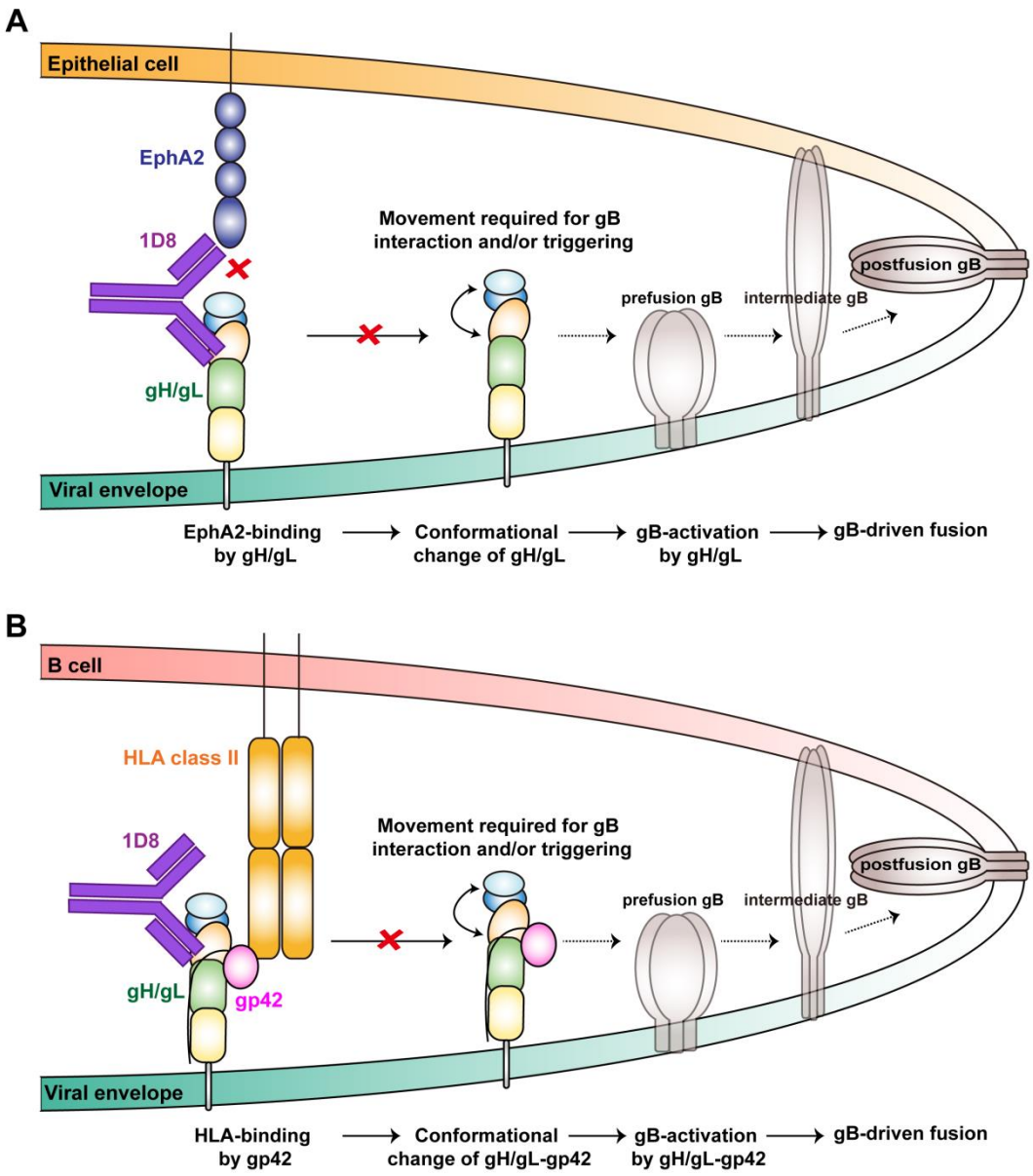

1013

1014

1015

1016

1017

1018

1019

SUPPLEMENTARY MATERIALS

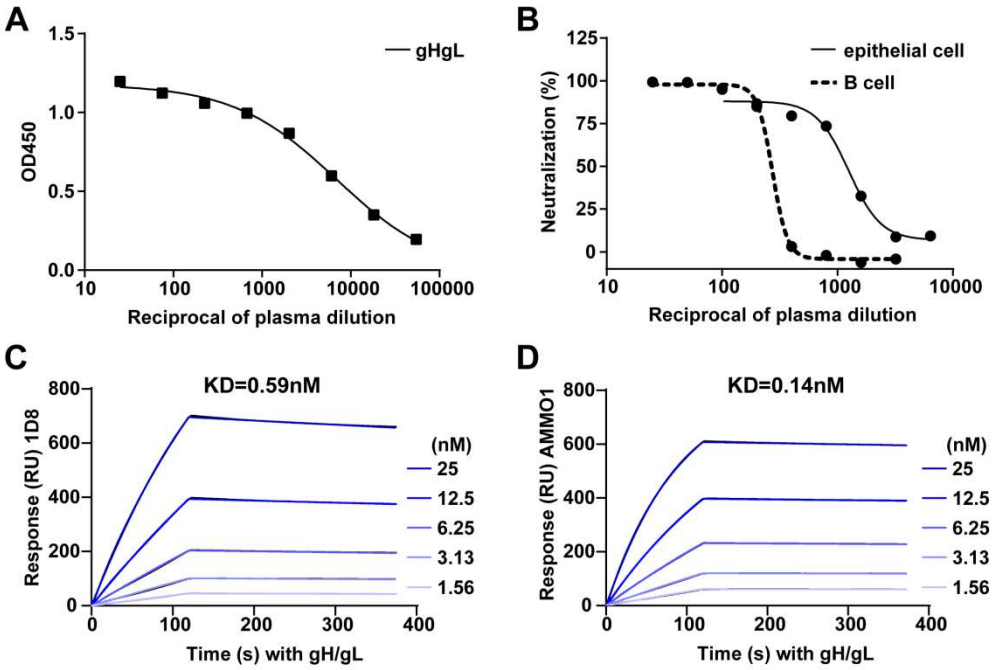

Fig. S1. Plasma binding and neutralizing activities from donor 27.

(A) Plasma binding activities to gH/gL measured by ELISA. (B) Plasma neutralizing activities against EBV infection of Raji B cells and HNE1 epithelial cells. Binding activity of 1D8 (C) or AMMO1 (D) to gH/gL measured by surface plasmon resonance (SPR). All experiments were performed in duplicate, and the data shown are means with SEM.

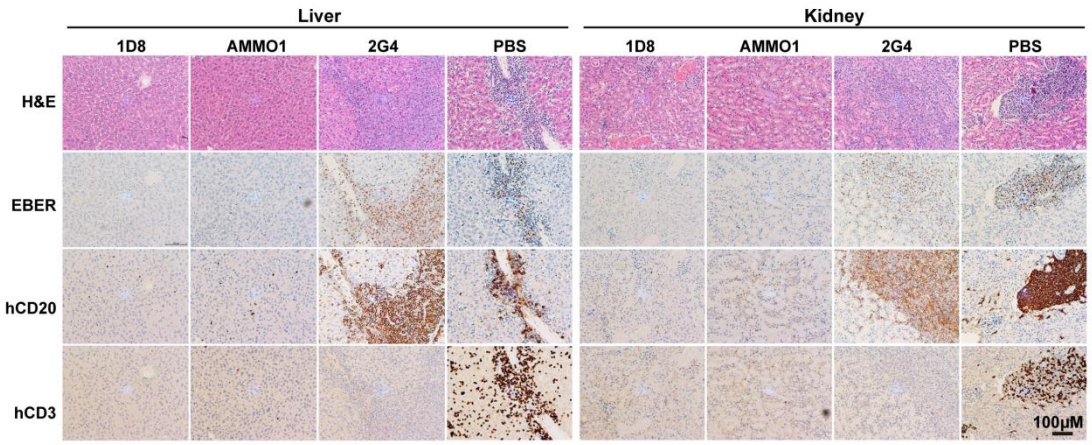

Fig. S2. 1D8 reduces viral replication and tissue damages in liver and kidney of mice.

Hepatic and renal sections stained for hematoxylin and eosin (H&E), human CD20 (hCD20), human CD3 (hCD3), and EBV encoded RNA (EBER) at necropsy. Scale bar of 100μm is shown.

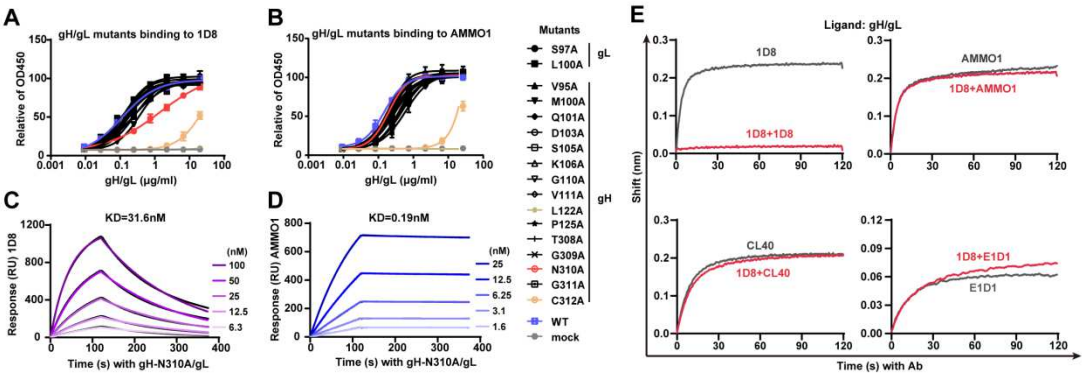

Fig. S3. Binding of 1D8 to gH/gL mutants and its competition with other gH/gL antibodies.

(A) 1D8 and (B) AMMO1 binding to various gH/gL mutants measured by ELISA. ELISA was performed in duplicate wells, and the data shown are means with SEM. Binding activity of 1D8 (C) and AMMO1 (D) to gH-N310A/gL mutant measured by surface plasmon resonance (SPR). (E) Competitive binding of 1D8 with AMMO1, CL40 or E1D1 to gH/gL measured by bio-layer interferometry (BLI).

Table S1. Neutralization potency of monoclonal antibodies.

Mab	Epithelial cells (μg/ml)		B cells (μg/ml)	
	IC_{50}	IC_{90}	IC_{50}	IC_{90}
1D8	0.123	0.187	0.238	0.442
2A6	0.745	2.270	1.320	＞50
AMMO1	0.127	0.305	0.318	1.148
2G4	NA	NA	NA	NA

Table S2. Kinetic Analysis of Antibodies Binding to gH/gL Measured by SPR.

Ligand	Anylate	kon (1/Ms) $\times 10^5$	koff (1/s) $\times 10^{-4}$	KD (nM)
1D8	gH/gL S97A	1.33	1.36	1.02
1D8	gH/gL L100A	1.07	1.55	1.44
1D8	gH V95A/gL	1.30	2.31	1.77
1D8	gH M100A/gL	1.51	1.96	1.30
1D8	gH Q101A/gL	0.95	1.95	2.03
1D8	gH D103A/gL	0.72	0.69	0.95
1D8	gH S105A/gL	0.90	0.97	1.08
1D8	gH K106A/gL	1.26	1.09	0.86
1D8	gH G110A/gL	2.66	0.26	0.10
1D8	gH V111A/gL	1.11	1.48	1.34
1D8	gH P125A/gL	0.71	2.00	2.79
1D8	gH T308A/gL	1.04	1.01	0.97
1D8	gH G309A/gL	0.95	0.95	1.00
1D8	gH N310A/gL	1.75	55.20	31.60
1D8	gH G311A/gL	0.78	2.05	2.62
1D8	gH/gL WT	2.45	1.46	0.59
AMMO1	gH N310A/gL	4.97	0.96	0.19
AMMO1	gH/gL WT	5.77	0.85	0.14

Table S3. Data collection and refinement statistics.

	EBV gH/gL-1D8
Data collection	
Space group	$P4_12_12$
Cell dimensions	
a, *b*, *c* (Å)	212.865, 212.865, 598.128
α, β, γ, (°)	90, 90, 90
Resolution (Å)	50.03-4.201(4.351-4.201) *
R_{sym} or R_{merge}	0.131 (1.261)
I / sI	8 (1.4)
Completeness (%)	99.34 (98.99)
Redundancy	8.1 (8.2)
Refinement	
Resolution (Å)	50.03-4.201
No. reflections	100331
R_{work} / R_{free}	23.31/26.77
No. atoms	
Protein	36304
B-factors	
Protein	161.73
R.m.s. deviations	
Bond lengths (Å)	0.009
Bond angles (°)	1.98
Ramachandran plot (%)	
Favored	91.48%
Allowed	7.06%
outlier	1.46%

One crystal was used.

*Values in parentheses are for highest-resolution shell.

Figures

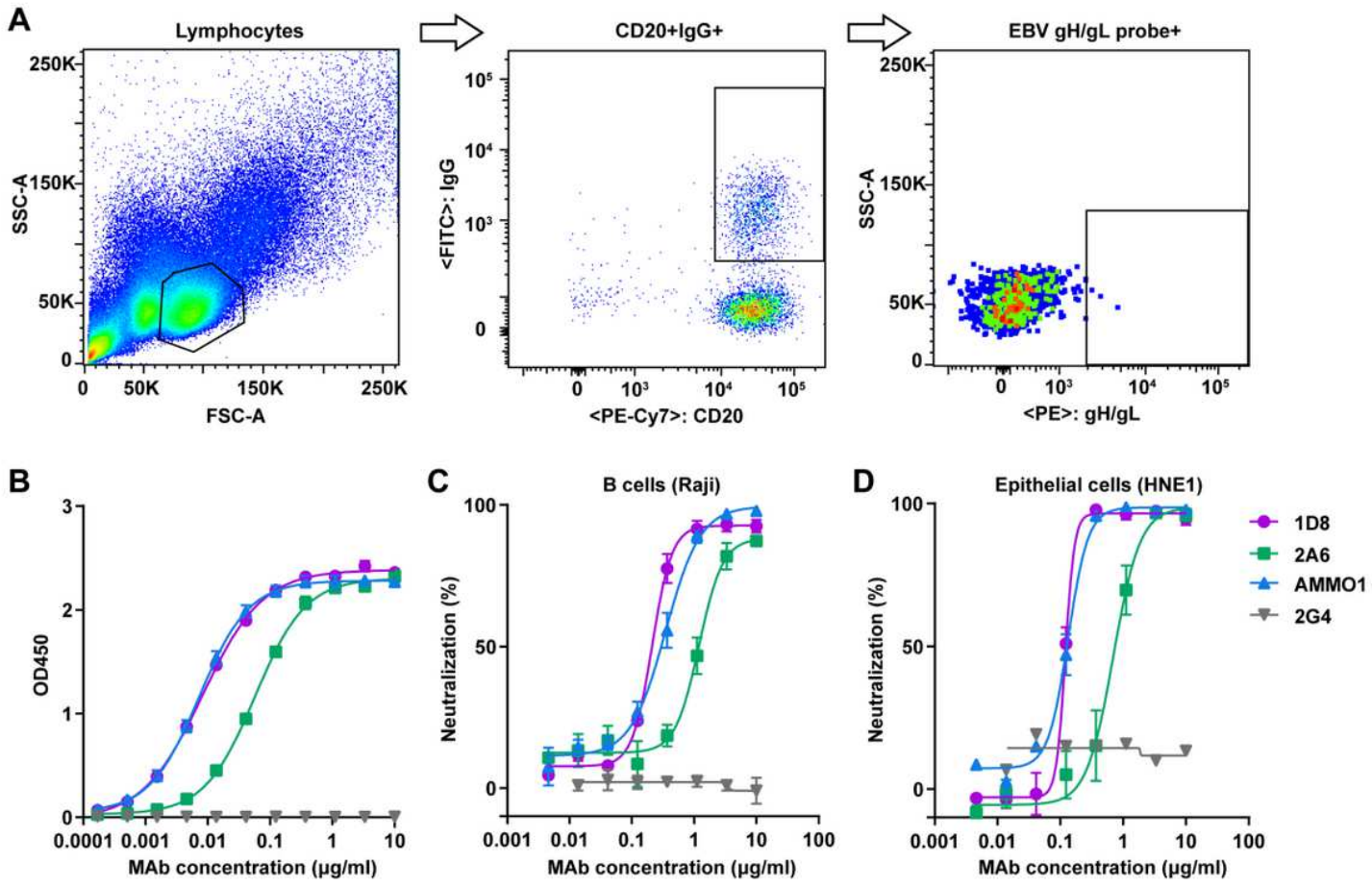

Figure 1

Isolation of gH/gL specific monoclonal antibodies using single B cell sorting and cloning A FACS based sorting strategy for gH/gL specific B cells. B Binding activities of 1D8 and 2A6, the positive control AMMO1, and the negative control 2G4 to EBV gH/gL measured by ELISA. The data are presented as means ± SEM. C Neutralizing activities of 1 D8 and 2A6, the positive control AMMO1, and the negative control 2G4 against EBV infection of Raji B cell lines and D HNE1 epithelia cell line. The data shown is means ± SEM. SSC A, side scatter area; FSC A, forward scatter area.

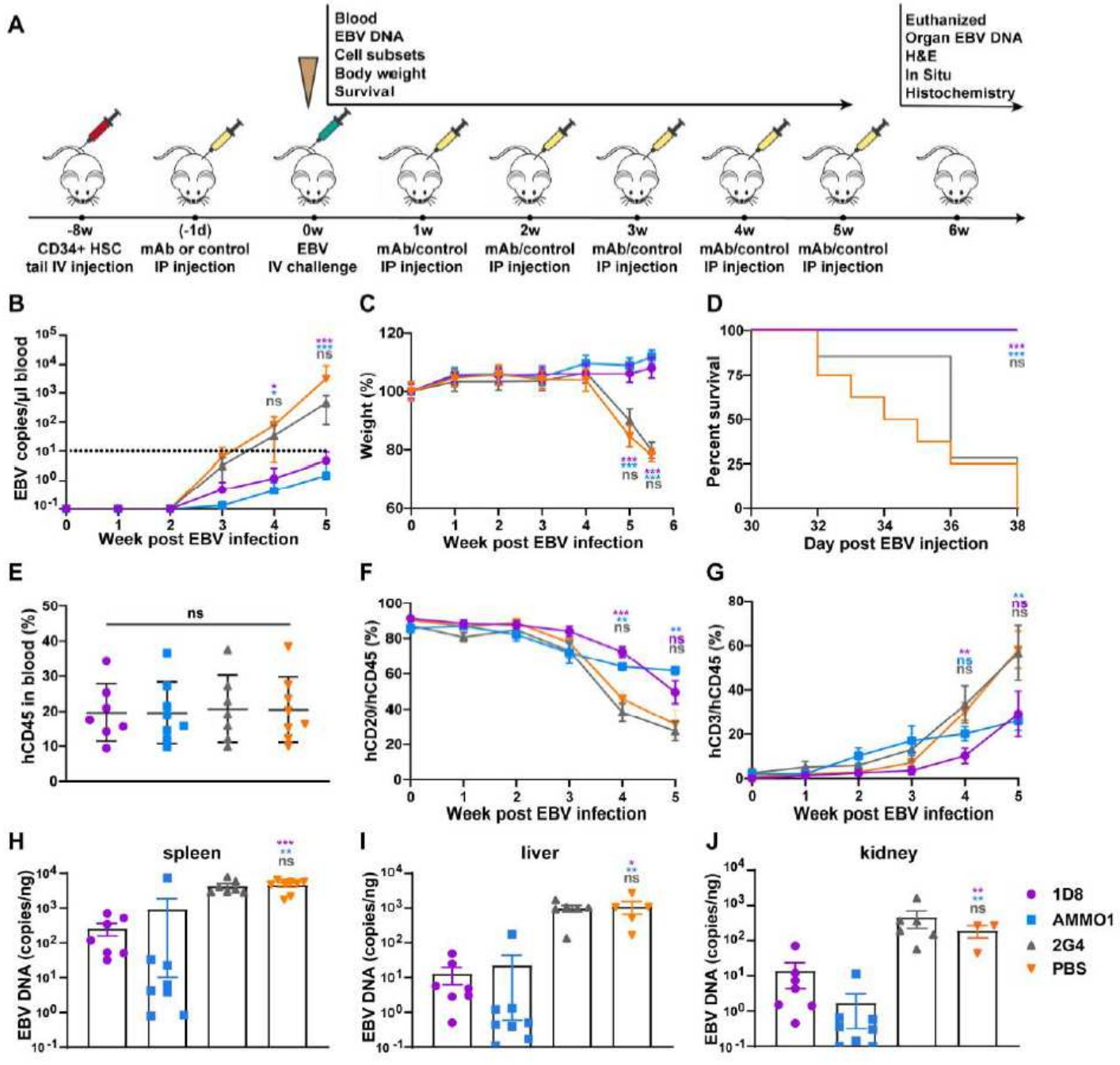

Figure 2

Protective effi cacy of 1D8 against lethal EBV challenge in humanized mice A Timeline for engrafting CD34+ human hematopoietic stem cells (HSC), antibody administration, viral challenge, and monitoring for various biological and clinical outcomes. Four hundred micrograms of 1D8, positive control AMMO1, negative control 2G4, or PBS negative control were administered to the humanized mice via intraperitoneal injection either 24h prior to or weekly for 5 weeks after intravenous challenge with Akata EBV. (B) EBV DNA in the peripheral blood, (C) body weight, and D) survival were monito red weekly. The percent changes in (E) hCD45+, F) hCD20+, or G) hCD3+ cells over the experiment period. On week 6 post infection, (H) virus titers in spleen, (I) liver, J) kidney were analyzed. All data are presented as mean ± SEM. *p < 0.05; **p < 0.01 ; ***p < 0.001; ns, no significant.

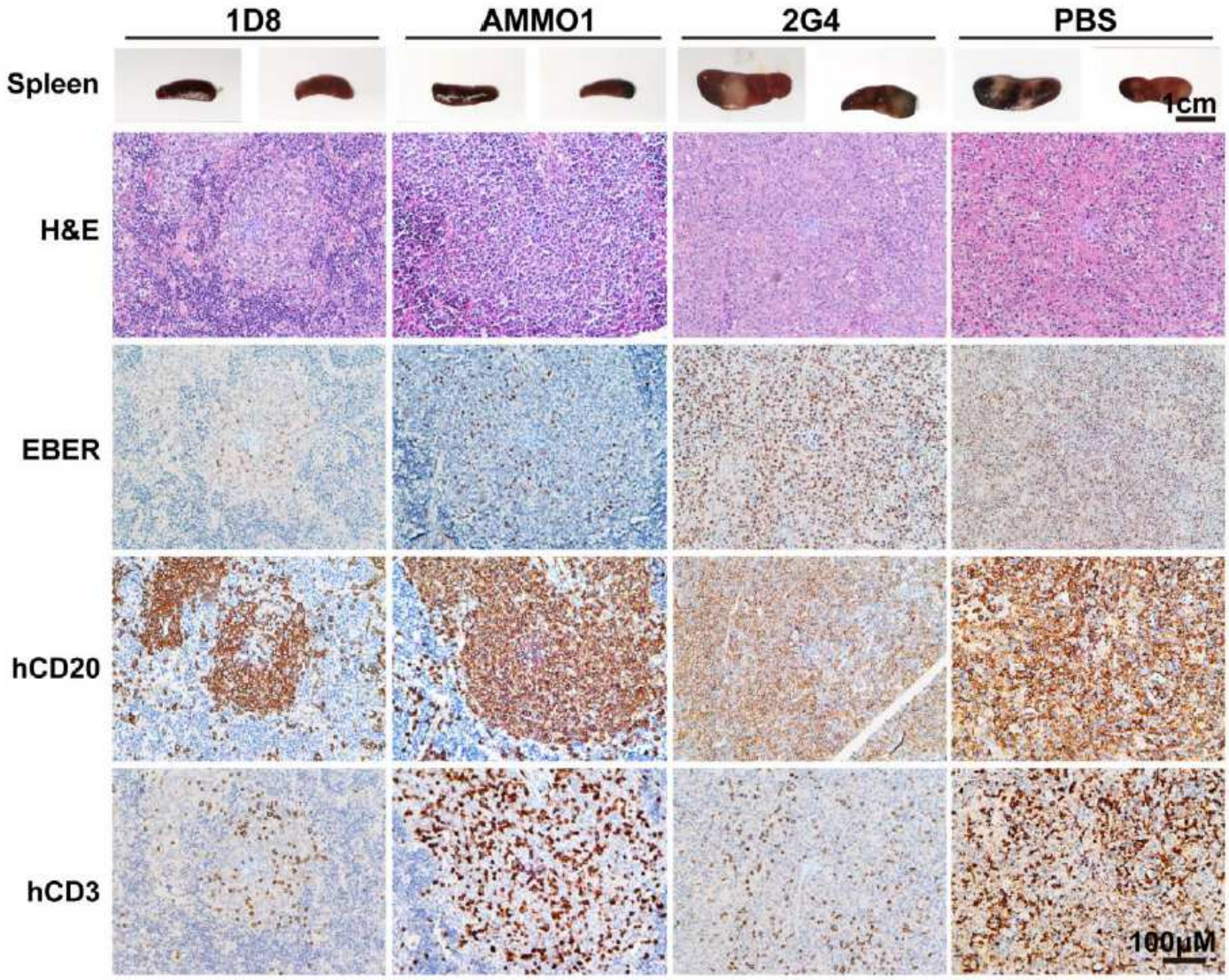

Figure 3

1D8 reduces viral replication and tissue damages in humanized mice Representative of macroscopic spleens and splenic sections stained for hematoxylin and eosin (H&E), EBV encoded RNA (EBER), human CD20 (and human CD3 (hCD3) at necropsy. The scale bars are indicated.

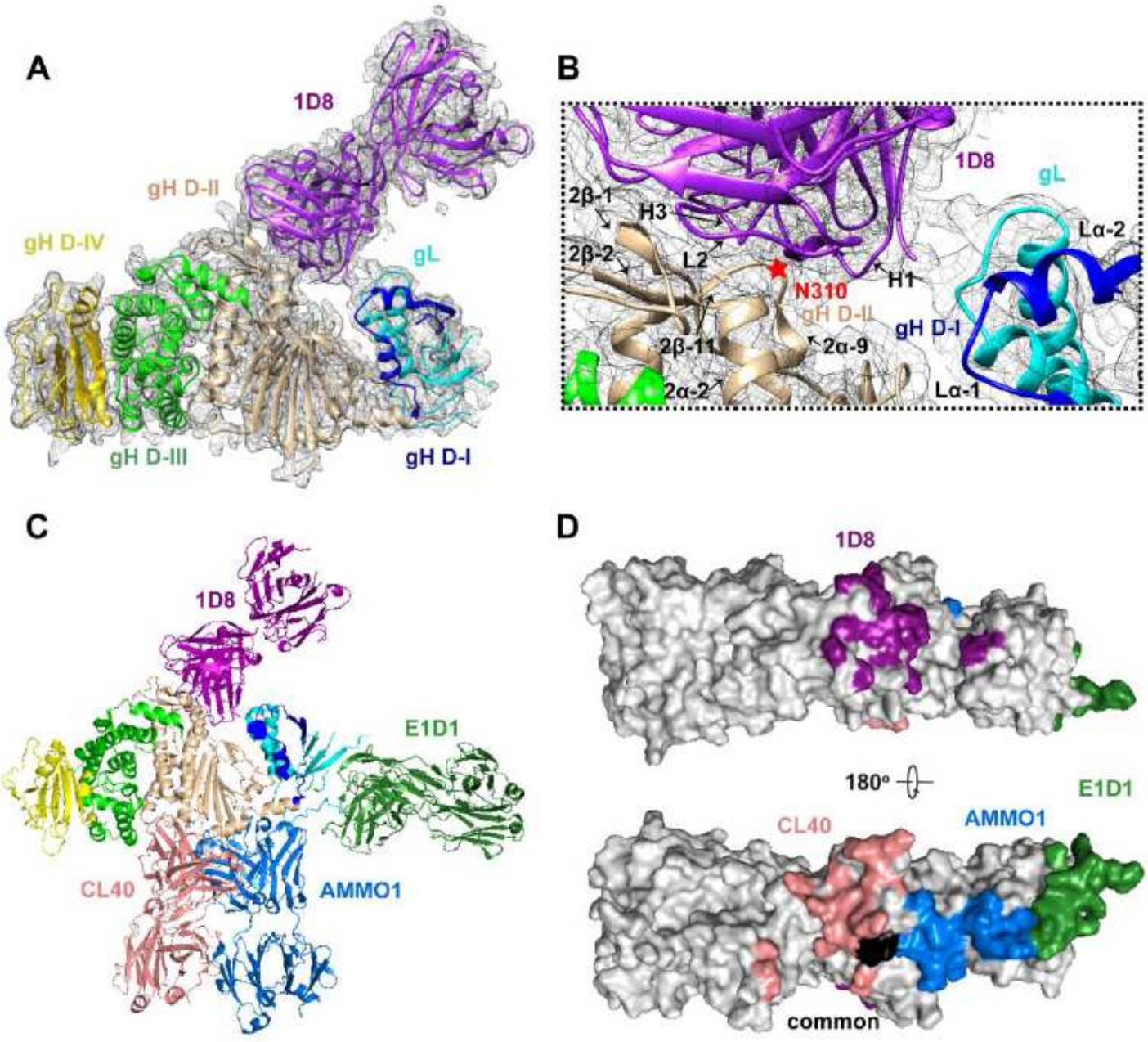

Figure 4

1D8 targets an unique epitope on gH/gL A Structure overview in a cartoon representation with gL in cyan, gH D I in blue, D II in wheat, D III in green, D IV in yellow, and 1D8 Fa b in purple. The map is contoured at 1.2 RMS to show the density. B Zoomed in view of the interaction between 1D8 and D I and D II. The key binding residue N310 of gH was indicated by a red star. C Cartoon representation of Fab 1D8 and other previously published Fabs AMMO1, CL40, and E1D1 bound to a single gH/gL molecule. The color scheme for gH/gL is as in (A) whereas 1D8 Fab in purple, AMMO1 Fab in light blue, CL40 Fab in pink, and E1D1 Fab in dar k green. D Surface mapping of the four Fab epitopes on gH/gL with the same color in C)). Areas in black indicate the region where structural change was found upon binding to AMMO1 or CL40.

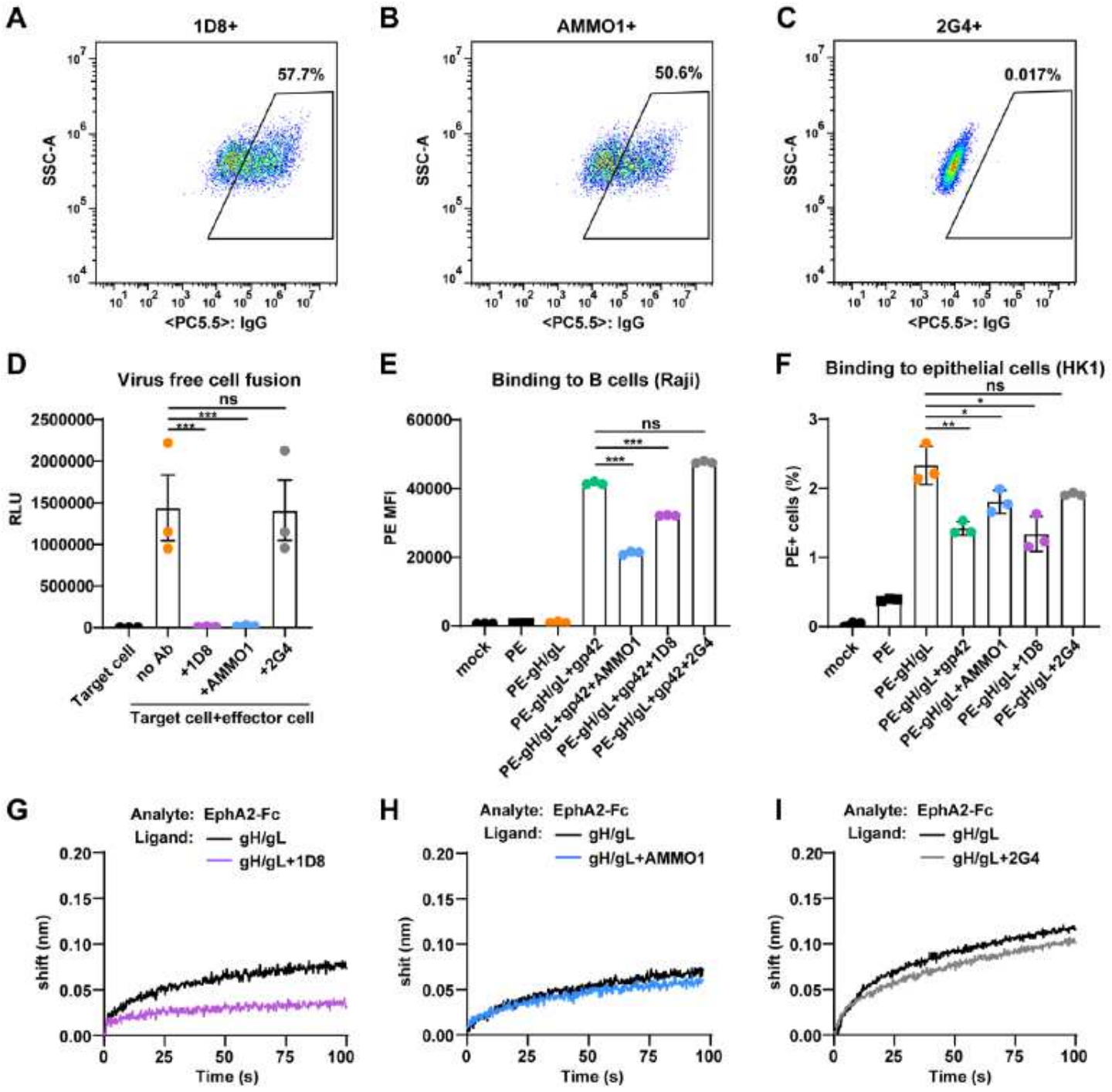

Figure 5

1D8 interferes with cell fusion and binding Quality control of gH/gL expression on the surface of CHO K1 cells by staining with 1D8 (A), positive control AMMO1 (B), and negative control 2G4 (C) before proceeded to the fusion experiment shown in (D). (D) Marked reduction in cell cell-cell fusion in the presence of 1D8, the positive control AMMMO1, but not the negative control 2G4. Marked reduction in gH/gL binding to Raji B cell (E) and HK1 epithelial cell (F) in the presence of 1D8, the positive control AM MO1 , but not the negative control 2G4. Binding of EphA1 EphA1-Fc to gH/gL was reduced by 1D8 (G), but not by AMMO1 (H) or 2G4 I) measured by Bio Bio-layer interferometry (BLI). All data are presented as

mean ± SEM. *p < 0.05; **p < 0.01; ***p < 0.001; ns, no significant. SSC SSC-A, side side-scatter area; PC5.5, PerCP PerCP-Cy5.5; RLU, relative light unit; SA SA-PE, streptavidin streptavidin-phycoerythrin; MFI, mean fluorescence intensity.

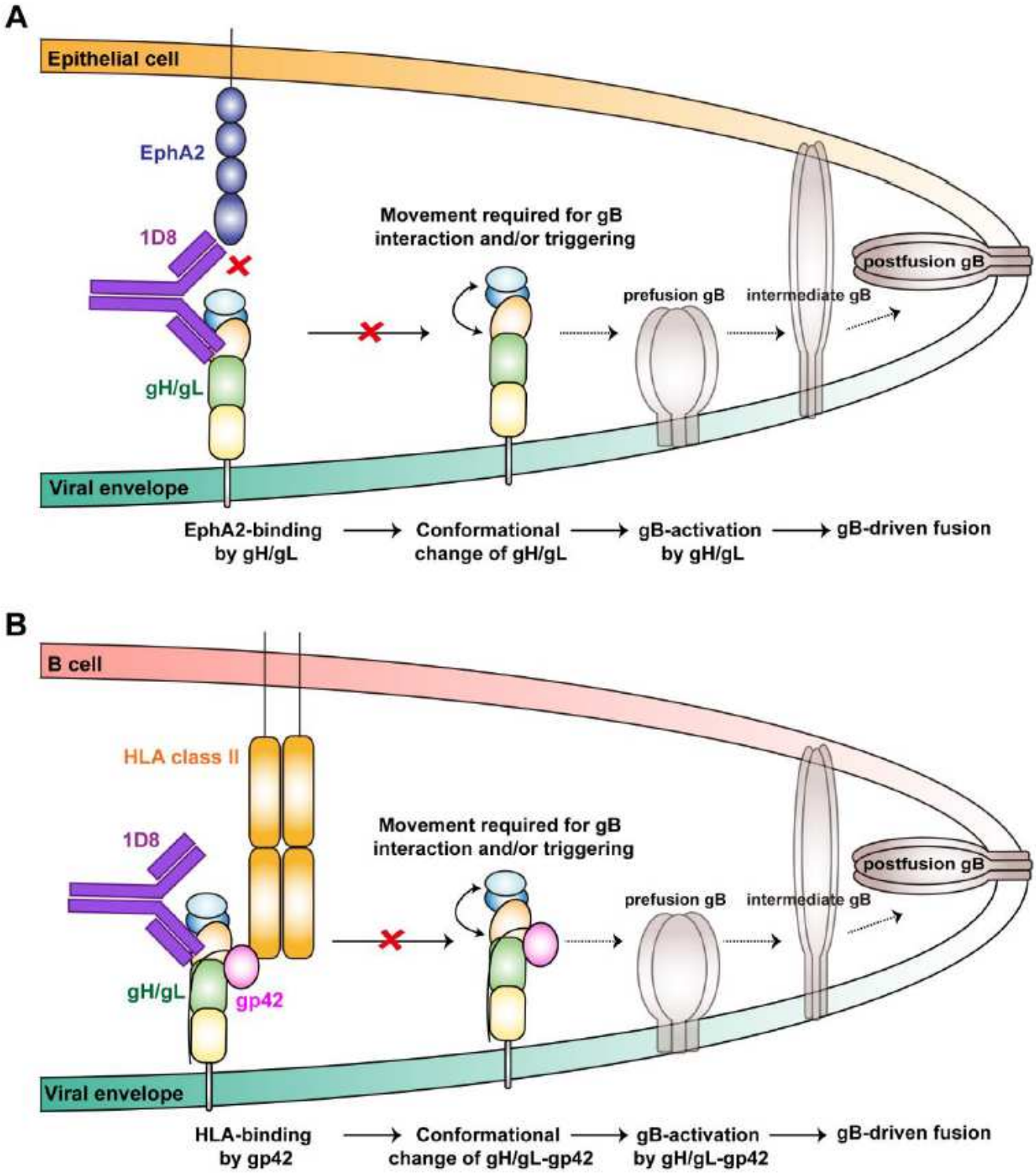

Figure 6

Possible mechanisms of 1D8 1D8-mediated neutralization neutralization. (A) For epithelia cells, 1D8 could interfere the interaction between gH/gL and EphA2 either by directly restricting access to the

interface or by indirectly posing allosteric hindrance. It could also restrict the movement across the D D-I/D -II groove of gH/gL t hat is required for gB interaction and triggering. (B) For B cells, 1D8 could also restrict the movement across the D D-I/D -II groove of gH/gL that is required for downstream viral entry. 1D8 does not appear influence interaction between gp42 and its recepto r HLA class II.